

A JOINT DENSITY FUNCTIONAL AND CLASSICAL MOLECULAR
DYNAMICS STUDY ON INTERFACE CHARACTERISTICS OF GRAPHENE
AND POLYETHERETHERKETONE

A THESIS SUBMITTED TO
THE GRADUATE SCHOOL OF NATURAL AND APPLIED SCIENCES
OF
MIDDLE EAST TECHNICAL UNIVERSITY

BY

ELIF SERT

IN PARTIAL FULFILLMENT OF THE REQUIREMENTS
FOR
THE DEGREE OF MASTER OF SCIENCE
IN
PHYSICS

SEPTEMBER 2020

Approval of the thesis:

**A JOINT DENSITY FUNCTIONAL AND CLASSICAL MOLECULAR
DYNAMICS STUDY ON INTERFACE CHARACTERISTICS OF
GRAPHENE AND POLYETHERETHERKETONE**

submitted by **ELIF SERT** in partial fulfillment of the requirements for the degree of
Master of Science in Physics Department, Middle East Technical University by,

Prof. Dr. Halil Kalıpçılar
Dean, Graduate School of **Natural and Applied Sciences**

Prof. Dr. Altuğ Özpineci
Head of Department, **Physics**

Assoc. Prof. Dr. Hande Toffoli
Supervisor, **Physics Department, METU**

Examining Committee Members:

Assoc. Prof. Dr. Engin Durgun
Institute of Material Science and Nanotechnology , Bilkent Uni.

Assoc. Prof. Dr. Hande Toffoli
Physics Department, METU

Assist. Prof. Dr. Osman Barış Malcıoğlu
Physics Department, METU

Date: _____

I hereby declare that all information in this document has been obtained and presented in accordance with academic rules and ethical conduct. I also declare that, as required by these rules and conduct, I have fully cited and referenced all material and results that are not original to this work.

Name, Surname: Elif Sert

Signature :

ABSTRACT

A JOINT DENSITY FUNCTIONAL AND CLASSICAL MOLECULAR DYNAMICS STUDY ON INTERFACE CHARACTERISTICS OF GRAPHENE AND POLYETHERETHERKETONE

Sert, Elif

M.S., Department of Physics

Supervisor: Assoc. Prof. Dr. Hande Toffoli

September 2020, 58 pages

Graphene is a single layer allotrope of carbon with a honeycomb arrangement of atoms, characterized by excellent mechanical properties such as high tensile strength, high Young's modulus as well as desirable electrical properties such as high electron mobility. Due to these superior properties, it is considered an important material in numerous technological applications. Among these, graphene-polymer composites have attracted significant interest in the materials research community in recent years. The use of these composites are particularly important in such fields as aeronautics where strength and low mass are simultaneously desirable. The testing, processing and construction of applicable mixtures of graphene and polymers pose challenges experimentally. Therefore, numerical modeling of graphene and graphene reinforced polymer composites is essential.

The main purpose of this thesis is to study the properties of the interface between graphene and the Poly Ether Ether Ketone (PEEK) polymer within the Density Functional Theory (DFT) and Molecular Dynamics (MD) frameworks. PEEK is a high performing thermoplastic polymer with remarkable mechanical characteristics, chem-

ical resistance, and relative high melting temperatures. We study the interaction from the smallest building units of a single monomer and build it up to 3-, 6- and 9-monomer chains, revealing all of its facets. In addition, we adhesion characteristics between graphene and PEEK oligomers as they slide past one another as a function of such important parameters as velocity, temperature and chain length.

Keywords: Graphene, Polymers, Interface, Density Functional Theory, Molecular Dynamics

ÖZ

GRAFEN VE POLİETERETERKETON ARAYÜZ KARAKTERİSTİKLERİNİN YOĞUNLUK FONKSİYONELİ VE MOLEKÜLER DİNAMİK ÇALIŞMASI

Sert, Elif

Yüksek Lisans, Fizik Bölümü

Tez Yöneticisi: Doç. Dr. Hande Toffoli

Eylül 2020 , 58 sayfa

Grafen, yüksek gerilme mukavemeti, yüksek Young modülü gibi mükemmel mekanik özelliklerin yanı sıra yüksek elektron hareketliliği gibi elektriksel özelliklerle karakterize edilen, atomların bal peteği düzenlemesine sahip tek katmanlı bir karbon allotropudur. Bu üstün özelliklerinden dolayı birçok teknolojik uygulamada önemli bir malzeme olarak kabul edilmektedir. Bunlar arasında grafen-polimer kompozitler, son yıllarda malzeme araştırma camiasında ilgi görmüştür. Bu kompozitlerin kullanımı, dayanıklılık ve düşük kütle için aynı anda mevcut olmasını gerektiren havacılık gibi alanlarda özellikle önemlidir. Uygulanabilir grafen ve polimer karışımlarının test edilmesi, işlenmesi ve yapımı deneysel olarak zorluklar oluşturmaktadır. Bu nedenle, grafen ve grafen takviyeli polimer kompozitlerin sayısal modellenmesi çok önemlidir.

Bu tezin temel amacı, grafen ile Poli Eter Eter Keton (PEEK) polimeri arasındaki arayüzün özelliklerini Yoğunluk Fonksiyonel Teorisi (DFT) ve Moleküler Dinamik (MD) çerçevelerinde incelemektir. PEEK, dikkat çekici mekanik özelliklere, kimyasal direnç ve görece yüksek erime sıcaklıklarına sahip yüksek performanslı bir ter-

moplastik polimerdir. Bu çalışmada, tek bir monomerin en küçük yapı birimlerinden gelen etkileşimlerinden başlayarak, 3, 6 ve 9 monomer zincirlerine kadar oluşturup tüm özelliklerini ortaya çıkarıyoruz. Buna ek olarak, hız, sıcaklık ve zincir uzunluğu gibi önemli parametrelerin bir fonksiyonu olarak grafen ve PEEK oligomerleri arasındaki yapışma karakteristiklerini birbirlerinin yanından geçerken görüyoruz.

Anahtar Kelimeler: Grafen, Polimer, Arayüz, Yoğunluk Fonksiyonelleri Teorisi, Moleküler Dinamik

To my dear family

ACKNOWLEDGMENTS

Firstly, I would like to express my deepest appreciation to my supervisor Assoc.Prof.Dr. Hande Toffoli who has the attitude and the substance of genius for her support, courage, trust and patience in this work. She continually inspired me to research and learn with her great education perspective. Without her understanding, help and guidance, this thesis would not have been possible. Additionally, I am very grateful to my co-supervisor Assoc.Prof.Dr.Ercan Gürses for employing me in his project and his polite, caring and informative attitude. I am very thankful to them for giving me the opportunity to study with them.

Also, I would like to thank Dr. Mine Konuk Onat, during the project and my thesis studies for sharing his knowledge and opinions about molecular dynamics calculations. Furthermore, I am very grateful to my project partners Dr.Hasan Gülaşık and Gözdenur Toraman for constantly discussions, suggestions and leading.

I also would like to thank the members of Computational Material Science Group especially Cem Maden and Gizem Özcan for their discussions and supportive attitude and friendship.

This work is financially supported by TÜBİTAK (The Science and Technological Research Council of Turkey)(Grant no:115M550)

TABLE OF CONTENTS

ABSTRACT	v
ÖZ	vii
ACKNOWLEDGMENTS	x
TABLE OF CONTENTS	xi
LIST OF TABLES	xiv
LIST OF FIGURES	xv
LIST OF ABBREVIATIONS	xviii
CHAPTERS	
1 INTRODUCTION	1
1.1 Graphene	2
1.2 PEEK Polymer	4
1.3 Graphene-Polymer Nanocomposites	4
1.4 Motivation	5
1.5 The Outline of the Thesis	6
2 METHODOLOGY	7
2.1 Density Functional Theory	7
2.1.1 Many-Particle Hamiltonian	7
2.1.2 Density Definiton	9

2.1.3	The Hohenberg-Kohn theorem	10
2.1.4	Energy in terms of density	10
2.1.5	Exchange-correlation energy	12
2.1.6	Kohn-Sham equations	13
2.1.7	van der Waals Corrections	14
2.2	Molecular Dynamics (MD)	15
2.2.1	The MD Technical issues	16
2.2.1.1	Verlet Algorithm	17
2.2.1.2	Velocity Verlet Algorithm	17
2.2.2	Interatomic Potentials	18
2.2.2.1	Lennard-Jones Potential	19
2.2.2.2	Adaptive Reactive Intermolecular Bond Order (AIREBO) Potential	20
2.2.2.3	Reactive Force Field (ReaxFF)	21
2.2.3	Thermodynamical Ensembles	21
2.2.3.1	Microcanonical (NVE) Ensemble	21
2.2.3.2	Canonical (NVT) Ensemble	22
2.2.3.3	Isothermal-Isobaric Ensemble	22
2.2.4	Temperature Control in MD Simulations	23
2.2.4.1	Velocity rescaling	23
2.2.4.2	Berendsen Thermostat	23
2.2.5	Molecular Dynamics using LAMMPS	24
2.2.5.1	The structure of a typical LAMMPS input	24

3	RESULTS AND DISCUSSION	27
3.1	DFT Results	27
3.1.1	Benchmark Calculations	27
3.1.2	Graphene-PEEK	28
3.2	MD Results	32
3.2.1	Benchmark Calculations	32
3.2.2	Graphene-PEEK monomer	32
3.2.3	Graphene and PEEK chains	35
3.2.4	Graphene-PEEK Polymer Sliding	41
4	CONCLUSION	49
	REFERENCES	51

LIST OF TABLES

TABLES

Table 3.1	Graphene lattice constant with DFT-D, DFT-DF and DFT-DF-C09 . . .	28
Table 3.2	Adsorption energies (eV/molecule) and adsorption distances (Å) of C ₇ H ₆ O ₂ , C ₆ H ₆ O ₂ and C ₆ H ₆ subunits on graphene. The values in boldface indicate the most stable orientations for each subunit.	31
Table 3.3	Adsorption energies (in eV) of sub-molecules on 6x6 graphene . . .	33
Table 3.4	Adsorption energies (in eV) of rod-like PEEK chains adsorbed on graphene as a function of temperatures	39
Table 3.5	Friction force between PEEK monomer and graphene as a function of velocity	43
Table 3.6	Friction force between graphene and N-chain PEEK molecules as a function of temperatures	46

LIST OF FIGURES

FIGURES

Figure 1.1	Honeycomb lattice structure of graphene sheet	2
Figure 1.2	Graphitic forms. Graphene is a 2-D building material with all other dimensionalities for carbon materials. It can be wrapped in buckyballs of 0-D, rolled in 1-D nanotubes or lined in 3-D graphite. Reprinted from [8]	3
Figure 1.3	PEEK chemical structure. Reprinted from [56]	5
Figure 2.1	Overview of dispersion correction in DFT. E_{KS} and V_{KS} correspond to Kohn-Sham total energies and potentials. Reprinted from [47]	15
Figure 2.2	Lennard-Jones potential function. Reprinted from [13]	19
Figure 3.1	Graphene lattice constant	28
Figure 3.2	Sub-units of PEEK. The carbons are gray, the hydrogens are white, and the oxygens are red.	29
Figure 3.3	Sub-units of PEEK as used in our calculations; $C_6H_6O_2$, $C_7H_6O_2$ and C_6H_6	29
Figure 3.4	Different configurations of C_6H_6	30
Figure 3.6	Different configurations of $C_7H_6O_2$	30
Figure 3.7	PEEK monomer on graphane	31
Figure 3.8	Graphene lattice constant using AIREBO	32

Figure 3.9	Final configurations front view of PEEK monomer on graphene at (a) 0K, (b) 100K and (c)300K	34
Figure 3.10	Final configurations side view of PEEK monomer at (a) 100K and (b) 300K	34
Figure 3.12	Initial configurations front view of (a) 3 PEEK, (b) 6 PEEK and (c) 9 PEEK on graphene	35
Figure 3.13	Final configurations of 3 monomer PEEK on graphene at different temperatures (a), (b), (c) side views and (d), (e), (f) are top views. . .	36
Figure 3.14	Final configurations of 6 monomer PEEK on graphene at different temperatures (a), (b), (c) side views and (d), (e), (f) are top views. . .	37
Figure 3.15	Final configurations of 9 monomer PEEK on graphene at different temperatures (a), (b), (c) side views and (d), (e), (f) are top views. . .	37
Figure 3.16	Adsorption energy graphs of 3 monomer PEEK on graphene at T=100K, T=300K and T=500K. Blue lines represent the energies taken every 10 ps during the last 100 ps of the simulation and red lines are averages.	38
Figure 3.17	The radius of gyration of the N-chain PEEK molecules on the graphene sheet for three different tempertures (a)3PEEK monomer,(b) 6 PEEK monomer, (c) 9 PEEK monomer	40
Figure 3.18	Linear distribution of N-chain PEEK molecules chains on graphene (a)3PEEK monomer,(b) 6 PEEK monomer, (c) 9 PEEK monomer . . .	41
Figure 3.19	A sketch of the Tomlinson model, The dashed lines indicates the periodic potential, and the particle is sketched as a triangle. Reprinted from [73]	42
Figure 3.20	Force on mobile atoms of 3 PEEK monomer during sliding with velocitied 1 m/s, 10 m/s and 100 m/s	43

Figure 3.21	Configurations of 3 PEEK molecules sliding with velocities of 1 m/s ,10 m/s and 100 m/s	44
Figure 3.22	Friction force on mobile atoms of 3 PEEK during sliding with velocities of 1m/s at 100K and 300K	45
Figure 3.23	Friction force on mobile atoms of 4 PEEK sliding with a velocity of 1 m/s at 1K, 100K and 300K	45
Figure 3.24	Friction force on mobile atoms of 5 PEEK sliding with a velocity of 1 m/s at 1K, 100K and 300K	45
Figure 3.25	Friction forces between N-chain PEEK molecules and graphene sheet as a function of temperature	46
Figure 3.26	Snapshots of N-chain PEEK molecules while sliding with a velocity of 1 m/s at 1K a) 3 PEEK, (b) 6 PEEK and (c) 9 PEEK on graphene on graphene	47

LIST OF ABBREVIATIONS

ABBREVIATIONS

2D	2 Dimensional
AFM	Atomic Force Microscopy
AIREBO	Adaptive Intermolecular Reactive Emprical Bond Order
CNT	Carbon Nanotube
DFT	Density Functional Theory
GGA	Generalized Gradient Aproximation
fs	femtosecond
LDA	Local Density Approximation
MD	Molecular Dynamics
ns	Nanosecond
PBE	Perdew-Burke-Ernzerhof
PEEK	Polyetheretherketone
ReaxFF	Reactive Force Field
Uni.	University

CHAPTER 1

INTRODUCTION

Many nanofillers, such as graphene and carbon nanotubes (CNT), have been extensively studied with the development of nano-science and technology to improve the mechanical, thermal and electrical properties of polymers. Among these, graphene promises to be more conducive to enhancing polymer matrix characteristics. Graphene and its derivatives have been integrated into a broad spectrum of polymers for multiple functional applications in recent years, including epoxy [1], polystyrene [2], polyethylene terephthalate [3], nylon [4] and polymethylmethacrylate (PMMA) [5]. Reinforcement of graphene and CNTs into polymer composites is important for the enhancing mechanical properties of them. The enhancement of the mechanical properties examined in graphene-polymer nanocomposites is usually due to the high specific surface area and graphene's excellent mechanical properties.[6]. On the other hand, understanding of adhesion between graphene and polymers is essential for graphene-based applications in nanocomposites and electronic devices [40]. In this thesis, the graphene-polymer interface behaviour is investigated.

In this chapter, the two components of our composites, namely the PEEK polymers and graphene, are introduced separately.

1.1 Graphene

Graphene, one of the carbon family's allotropes, is a planar monolayer of sp^2 hybridized carbon atoms arranged in a 2-D lattice and its unit cell is a two-dimensional rhombus as depicted in Fig. 1.1

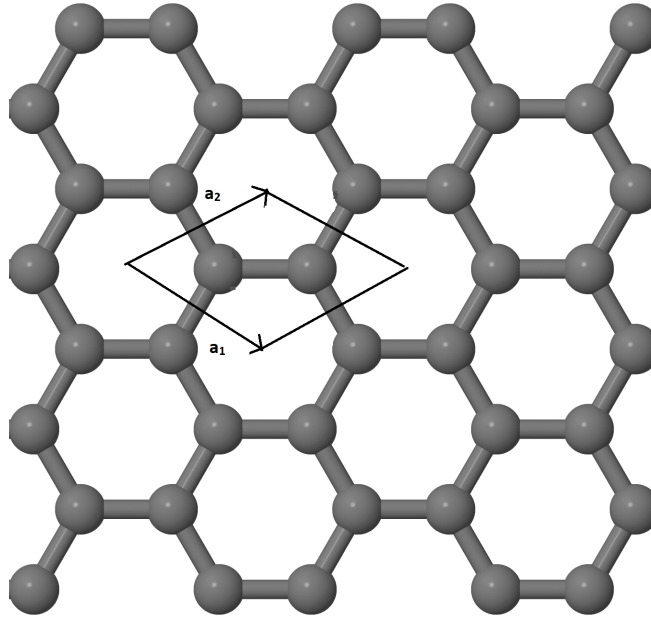


Figure 1.1: Honeycomb lattice structure of graphene sheet

A honeycomb lattice is an hexagonal lattice with a basis of two atoms in each unit cell. If a is the distance between nearest neighbors, the primitive lattice vectors can be written as

$$\vec{a}_1 = \frac{a}{2} (3, \sqrt{3}) \quad (1.1)$$

$$\vec{a}_2 = \frac{a}{2} (3, -\sqrt{3}) . \quad (1.2)$$

Graphene was known as the basic construction block for all other dimensional carbon materials [7]. For example, CNTs (1-D carbon allotropes) can be created by rolling a graphene nanoribbon into a cylinder. Graphite (3-D carbon allotrope) is composed of sheets of graphene stacked on top of each other as can be seen in Fig. 1.2

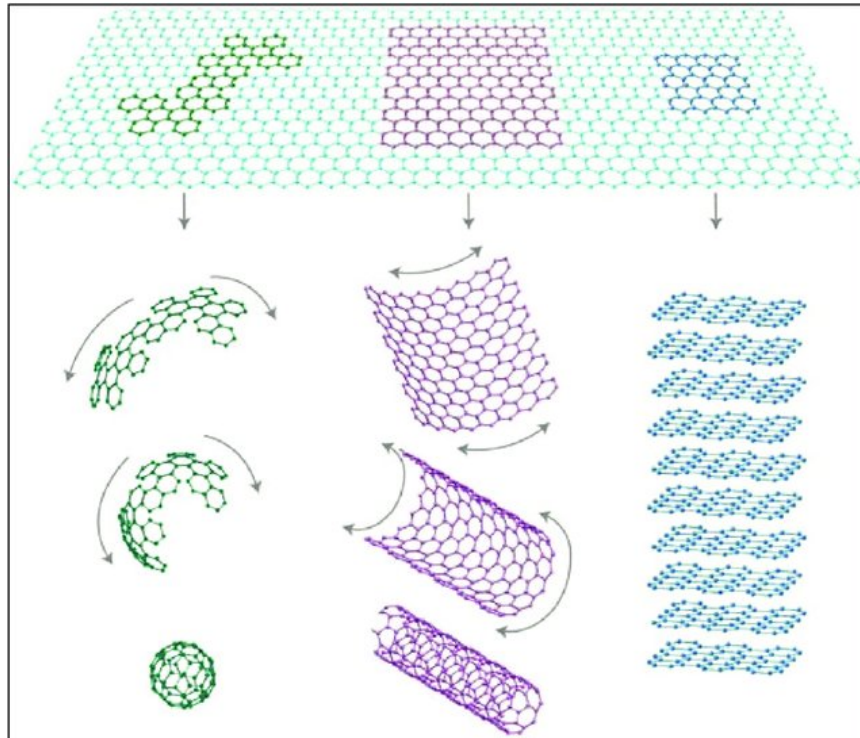


Figure 1.2: Graphitic forms. Graphene is a 2-D building material with all other dimensionalities for carbon materials. It can be wrapped in buckyballs of 0-D, rolled in 1-D nanotubes or lined in 3-D graphite. Reprinted from [8]

Graphene has many mechanical, thermal and electrical characteristics such as high carrier mobility under ambient condition ($250,000 \text{ cm}^2\text{V}^{-1}\text{s}^{-1}$) [7] [9], exceptional thermal conductivity and excellent mechanical properties with Young's modulus of 1 TPa [8]. Based on these favoured properties, graphene finds its applications in various fields such as sensors, solar cells, energy storage devices and nanocomposites [45]. For example, adding 1 volume per cent graphene into polystyrene, the nanocomposite has conductivity of 0.1 Sm^{-1} which is used in many electrical applications [10] [45]. Another example is that inclusion of graphene into PVA increase the mechanical characteristic such as Young modulus [11]. Therefore, nanocomposites of graphene-polymer have shown great potential to act as functional materials.

Also, a moire pattern forms when two graphene are overlaid with a relative twist. When the electronic structure of the system is studied, at a specific angle of about 1.1 degrees which is called as magic angle the system exhibit flat bands near zero Fermi energy resulting in correlated insulating states at half-filling [67] [68]. In conclusion,

this twisted bilayer graphene can exhibit alternating superconducting and insulating regions [69].

1.2 PEEK Polymer

Polymers are large molecules that consist of series of bonding building blocks called as monomers. Many polymer groups consist of hydrocarbons, carbon compounds and hydrogen. Such polymers are made mainly of carbon atoms bound together in long chains which are considered as the polymer's backbone. Examples of such are polyethylene, polypropylene, polystyrene and polymethylpentene. Also, there are polymers that contains elements other than carbon in their backbones. For example, nylons include nitrogen atoms in the backbone of the repeated structures and polyesters contain oxygen in the backbone. Furthermore, there are polymers that are considered as inorganic due to having inorganic elements such as silicon on their backbones.

In this study, we choose polyetheretherketone (PEEK) which the chemical structure is given in ???. It is a high-performance, semi-crystalline, colorless thermoplastic with excellent mechanical properties. It has Young's modulus of elasticity is 3.6 GPa and its tensile strength is 170 MPa [16]. In addition, PEEK is used as frictional coatings for high pressure and high ambient temperatures due to its excellent tribological properties [17]. Thanks to many superior properties of PEEK and its composites, they are widely used in electrical, biomedical, automotive and aerospace applications. For instance, PEEK and its composites are replacing aluminium alloys in many structural parts in aerospace industry [57]. Based on the properties before, PEEK is selected as our material to study the interface characteristics with graphene.

1.3 Graphene-Polymer Nanocomposites

Nanocomposite properties are determined by the properties of components, composition, structure and interfacial interactions. For example, properties of graphene based nanocomposite are investigated by modeling the graphene at atomic scale and con-

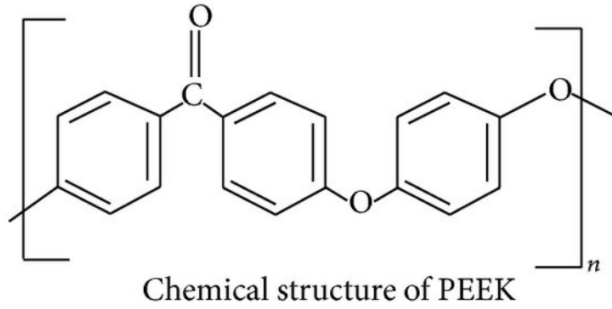


Figure 1.3: PEEK chemical structure. Reprinted from [56]

sidering a hybrid interphase between graphene and epoxy [58]. The interaction between graphene and polymer composites can be covalently [60] and non-covalently [61]. Particularly, the non-covalent functionalization depends on hydrogen bonding $\pi - \pi$ stacking [46]. Generally, in non-covalently functionalized graphene-polymer nanocomposites, the interfacial interactions consist of Van der Waals forces that are weaker than covalent bonds [62]. The interfacial adhesion characteristic plays an important role for determining the improvements in mechanical properties of graphene and its derivatives based polymer nanocomposites [35] [59]. For example, pullout process of graphene from an epoxy/graphene composite filled with a CNT in order to calculate interaction energy and interfacial adhesion between the graphene and epoxy matrix showed that the addition of a CNT strengthens the interfacial adhesion between graphene and polymer matrix [36].

1.4 Motivation

The interface between polymers and graphene has been investigated at multiple scales from coarse-grained methods [70] to quantum mechanical methods such as density functional theory (DFT) [71]. In this study, we investigated the interface properties of graphene and PEEK polymer by starting with smallest aromatic rings. Studying from the isolated rings gives us a understanding the relative effect of each ring with respect to the others. Later, we investigated the interface with single PEEK monomer and longer PEEK chains. This is the first study on this interface with a larger spectrum of relevant variables.

1.5 The Outline of the Thesis

In the first chapter of this thesis, graphene/polymer nanocomposites, graphene and polymer that we decided to PEEK is introduced. In the second chapter, the methods are introduced which we used while studying interfacial characteristics of graphene and PEEK. In the third chapter, the results obtained from our DFT and MD simulations is given and the final chapter is conclusion.

CHAPTER 2

METHODOLOGY

2.1 Density Functional Theory

Density functional theory (DFT) is an ab initio methods for solving the nonrelativistic, time-independent Schrödinger equation. It provides a powerful tool to compute the quantum states of atoms, molecules and solids. In DFT, the ground state energy of a system can be computed from the electron density.

Thomas Fermi theory [42] has been used to compute the total energy of a system based on electron density since the early 1920s. However, its accuracy is limited by some errors because of negligent representation of exchange energy and lack of electron correlation. For many electron systems such as molecules and solids, modern DFT offers better predictions[63].

2.1.1 Many-Particle Hamiltonian

In quantum mechanics, the Hamiltonian is the operator corresponding to the total energy of the system which is the sum of kinetic energy and potential energy

$$\hat{H} = \hat{T} + \hat{V}. \quad (2.1)$$

There are energy contributions due to two kinds of particles into the Hamiltonian; electrons and nuclei. There are three types of interactions between these components contribute to the potential \hat{V} ;

Nucleus-nucleus interaction : Nucleus are taken as classical particles that interact

via Coloumbic forces.

Nucleus-electron interaction : This is a coulombic interaction involving one electron at a time. Electrons are considered as quantum mechanical particles, so this interaction behaves like an external single-body potential acting on electrons.

Electron-electron interaction : This is a coulombic interaction involving pairs of electrons.

For a system with N_n nuclei and N_e electrons, the Hamiltonian can be written as

$$\hat{H} = \hat{T}_e + \hat{T}_n + \hat{V}_{en} + \hat{V}_{ee} + \hat{V}_{nn}. \quad (2.2)$$

Total kinetic energy operator is the sum of the kinetic energies of the electrons and nuclei. However, as the ions are heavier than electrons several tens of thousands of times, their contributions to kinetic energy are overlooked and this approximation is called Born-Oppenheimer approximation.[33]

The Born-Oppenheimer approximation [33] allows to separate the motion of nuclei and electrons. Since the mass of the nuclei is much larger than the mass of electron, nuclei move more slowly than electrons. Therefore, the many body Hamiltonian becomes

$$\hat{H} = \hat{T}_e + \hat{V}_{ne} + \hat{V}_{ee} + \hat{V}_{nn}. \quad (2.3)$$

Here, the first term is the kinetic energy operator, second term is the interaction between electrons and nuclei, the third term is the interaction between electrons such that electrons are moving under influence of a screened potential and the last term is the classical nucleus-nucleus interaction.

In extended form;

$$\hat{H} = \frac{-\hbar^2}{2m} \sum_i^{N_e} \nabla_i^2 + \frac{e^2}{4\pi\epsilon_0} \left[- \sum_i^{N_e} \sum_I^{N_n} \frac{Z_I}{|\vec{r}_i - \vec{R}_I|} + \frac{1}{2} \sum_i^{N_e} \sum_{j \neq i}^{N_e} \frac{1}{|\vec{r}_i - \vec{r}_j|} \frac{1}{2} \sum_I^{N_n} \sum_{J \neq I}^{N_n} \frac{Z_I Z_J}{|\vec{r}_I - \vec{r}_J|} \right]. \quad (2.4)$$

where \hbar is the Planck's constant, m is the mass of electron, Z is the nuclear charge, \vec{r} is the position of the electron and \vec{R} is the position of the nuclei.

Here also, indices i and j run through electrons and I and J run over nuclei.

Whether our system is an atom, a molecule or a solid is dependent on \hat{V}_{ne} and \hat{V}_{nn} .

In the equation above, many-body Hamiltonian is written in SI units. A more natural unit system for this problem is atomic units. In the atomic unit system, the energy and length are measured in terms Hartree which is the the ground state energy of the electron in the hydrogen atom and the Bohr radius (a_0) that average ground state radius respectively. In atomic units, the Hamiltonian becomes

$$H = \frac{-1}{2} \sum_i^{N_e} \nabla_i^2 - \sum_i^{N_e} \sum_I^{N_n} \frac{Z_I}{|\vec{r}_i - \vec{R}_I|} + \frac{1}{2} \sum_i^{N_e} \sum_{j \neq i}^{N_e} \frac{1}{|\vec{r}_i - \vec{r}_j|} + \frac{1}{2} \sum_I^{N_n} \sum_{J \neq I}^{N_n} \frac{Z_I Z_J}{|\vec{R}_I - \vec{R}_J|}. \quad (2.5)$$

The usual quantum-mechanical approach to Schrödinger's equation is that one specifies the system by choosing \hat{V} in Eq. (2.2), plug it into the Schrödinger equation, solve the wave function equation and then determine the observables by taking expectation values of operators with this wave function. The particle density is one of the observables calculated in this way.

2.1.2 Density Definiton

Density operator is a measure of contribution from each electron and defined as

$$\hat{n} = \sum_i \delta(\vec{r} - \vec{r}_i). \quad (2.6)$$

We take the expectation value of the density operator, since it is corresponds to the observable

$$\langle \psi | \hat{n} | \psi \rangle = \sum_i \int |\psi(\vec{r}_1 \dots \vec{r}_N)|^2 \delta(\vec{r} - \vec{r}_i) d\vec{r}_1 \dots d\vec{r}_N \quad (2.7)$$

$$= N \int |\psi(\vec{r}_1 \dots \vec{r}_N)|^2 d\vec{r}_2 d\vec{r}_3 \dots d\vec{r}_N. \quad (2.8)$$

Here, by integrating density over all space gives total number of electrons.

$$\int n(\vec{r})d\vec{r} = N. \quad (2.9)$$

2.1.3 The Hohenberg-Kohn theorem

DFT is made possible by the existence of two theorems proposed and demonstrated by Hohenberg and Kohn in 1964 [12]. The first theorem is that for any system of interacting particles in an external potential $V_{ext}(r)$, the density is uniquely determined. It proves that there is a one to one correspondence between the external potential and the ground state densities in many electron systems. The second theorem states that a universal functional for the energy $E(n)$ can be defined in terms of the density and the exact ground state is the global minimum value of this functional. Therefore, one can find the total energy of the ground state by minimizing with respect to \vec{r} . Then the density that minimizes the energy is the ground state density.

2.1.4 Energy in terms of density

In order to minimize the electronic energy with respect to the density, first step is to write the total energy in term of density.

The the expectation value of the nuclei-electron interaction

$$\langle \psi | \hat{V}_{ne} | \psi \rangle = - \sum_i^{N_e} \sum_I^{N_n} \int \psi^*(\vec{r}_1 \dots \vec{r}_N) \frac{Z_I}{|\vec{r}_i - \vec{R}_I|} \psi(\vec{r}_1 \dots \vec{r}_N) d\vec{r}_1 \dots d\vec{r}_N \quad (2.10)$$

By collecting wavefunction under norm square we get

$$\langle \psi | \hat{V}_{ne} | \psi \rangle = - \sum_i^{N_e} \sum_I^{N_n} \int |\psi(\vec{r}_1, \dots, \vec{r}_n)|^2 d\vec{r}_1 \dots d\vec{r}_N. \quad (2.11)$$

and by expanding the sum over index i

$$\begin{aligned} \langle \psi | (\hat{V}_{ne}) | \psi \rangle = & - \sum_I^{N_n} \left[\int \frac{Z_I}{|\vec{r}_1 - \vec{R}_I|} |\psi(\vec{r}_1, \dots, \vec{r}_n)|^2 d\vec{r}_1 \dots d\vec{r}_N \right. \\ & \left. + \int \frac{Z_I}{|\vec{r}_2 - \vec{R}_I|} |\psi(\vec{r}_1, \dots, \vec{r}_n)|^2 d\vec{r}_1 \dots d\vec{r}_N + \dots \right]. \end{aligned} \quad (2.12)$$

Similarly, the expectation value of electron-nuclei interaction energy

$$\langle \psi | \hat{V}_{ne} | \psi \rangle = -\frac{1}{N_e} \sum_I^{N_n} \left[\int \frac{Z_I}{|\vec{r}_1 - \vec{R}_I|} n(\vec{r}_1) + \int \frac{Z_I}{|\vec{r}_2 - \vec{R}_I|} n(\vec{r}_2) + \dots \right]. \quad (2.13)$$

Here, dummy variables can be replaced so that electron-nuclei interaction can be written as

$$E_{ne} = - \sum_I^{N_n} \int n(\vec{r}) \frac{Z_I}{|\vec{r} - \vec{R}_I|} d\vec{r} = \int n(\vec{r}) V_{ne}(\vec{r}) d\vec{r}. \quad (2.14)$$

Electron-electron interaction cannot be written in terms of the single-particle density but instead only in terms of the two-particle density

$$E_{ee} = \frac{1}{2} \int \int d\vec{r} d\vec{r}' \frac{n^{(2)}(\vec{r}, \vec{r}')}{|\vec{r} - \vec{r}'|}. \quad (2.15)$$

Here, $n^{(2)}$ can be expressed as the probability that an electron exist at point \vec{r} given that a second electron exists at point \vec{r}' . However, the method does not allow for the use of such a two-particle density but instead only the one-particle density. Therefore, there is an approximation such that if two electrons are uncorrelated then two-particle density can be expressed as the product of one particle densities. We can write $n^{(2)}$ in terms of one-particle densities and a correction

$$n^{(2)}(\vec{r}, \vec{r}') = n(\vec{r})n(\vec{r}') + \Delta n^{(2)}(\vec{r}, \vec{r}'). \quad (2.16)$$

so the electron-electron interaction can be written as

$$E_{ee} = \frac{1}{2} \int \int d\vec{r} d\vec{r}' \frac{n^{(2)}(\vec{r}, \vec{r}')}{|\vec{r} - \vec{r}'|} + \Delta E_{ee}. \quad (2.17)$$

where ΔE_{ee} is the difference in the electronic energy between the correlated and uncorrelated systems.

The kinetic energy term cannot be written easily because it contains a derivative term. In order to handle the kinetic energy term, there is one of the key assumption of DFT which that the density can be written as the sum norm squares of a collection of single-particle orbitals

$$\hat{n}(\vec{r}) = \sum_n^{N_e} |\phi(\vec{r})|^2. \quad (2.18)$$

These orbitals are called Kohn-Sham orbitals and they are initially unspecified. The kinetic energy is written as the sum of the kinetic energies of the Kohn-Sham orbitals. However, this is not equal to the kinetic energy of the real many-particle system. Therefore, the kinetic energy can be expressed as the single-particle kinetic energy plus a correction

$$\hat{T} = \frac{-1}{2} \sum_n^{N_e} \int d\vec{r} \phi_n^*(\vec{r}) \nabla^2 \phi_n(\vec{r}) d\vec{r} + \Delta T. \quad (2.19)$$

By putting all of the interactions in terms of density, the total energy can be written as

$$E = \frac{-1}{2} \sum_n^{N_e} \int d\vec{r} \psi_n^*(\vec{r}) \nabla^2 \psi_n(\vec{r}) d\vec{r} + \int n(\vec{r}) V_{ne}(\vec{r}) d\vec{r} + \frac{1}{2} \int \int d\vec{r} d\vec{r}' \frac{n^{(2)}(\vec{r}, \vec{r}')}{|\vec{r} - \vec{r}'|} + \Delta T + \Delta E_{ee}. \quad (2.20)$$

In the equation, the sum of last two terms are called as exchange-correlation energy. The quality of a DFT calculation is determined by how close the approximate exchange and correlation comes to the exact value :

$$E_{xc} = \Delta E_{ee} + \Delta T. \quad (2.21)$$

2.1.5 Exchange-correlation energy

The origin of exchange energy is the Pauli repulsion and the origin of the correlation energy is the repulsion between electrons. There are several approximation for this sum, one of them is the local-density approximation (LDA) [40] which is

$$E_{xc} = \int d\vec{r} n(\vec{r}) \epsilon_{xc}(n). \quad (2.22)$$

where $\epsilon_{xc}(n)$ is a simple function of n . Within the local approximation, the total energy may be written as

$$E = \frac{-1}{2} \sum_n^{N_e} \int d\vec{r} \psi_n^*(\vec{r}) \nabla^2 \psi_n(\vec{r}) d\vec{r} + \int n(\vec{r}) V_{ne}(\vec{r}) d\vec{r} + \frac{1}{2} \int \int d\vec{r} d\vec{r}' \frac{n^{(2)}(\vec{r}, \vec{r}')}{|\vec{r} - \vec{r}'|} + \int d\vec{r} n(\vec{r}) \epsilon_{xc}(n). \quad (2.23)$$

However, the density is considered as constant in LDA approximation. Because of the cancellation of errors, it underestimate the exchange energy and overestimate the correlation energy [49]. Because of this, exchange-correlation energy is expanded in terms of gradient of the density and it is referred as generalized gradient approximation (GGA) [50].

2.1.6 Kohn-Sham equations

Using the Hohenberg-Kohn Theorems described in section 2.1.3, we minimize the total energy in order to obtain the orbitals that produce the energy of the ground state. Functional derivative gives :

$$\frac{\delta E_e}{\delta \phi_i^*(\vec{r})} = \frac{\delta T_s}{\delta \phi_i^*(\vec{r})} + \left[\frac{\delta E_{ext}}{\delta n(\vec{r})} + \frac{\delta E_{Hartree}}{\delta n(\vec{r})} + \frac{\delta E_{xc}}{\delta n(\vec{r})} \right] \frac{\delta n(\vec{r})}{\delta \phi_i^*(\vec{r})} = \epsilon_i \phi_i(\vec{r}). \quad (2.24)$$

by applying the orthonormality condition of the Kohn-Sham orbitals, obtain an equation resemble a Schrödinger equation :

$$[\hat{T} + V_H + V_{xc} + V_{ext}] \phi_i(\vec{r}) = \epsilon_i \phi_i(\vec{r}). \quad (2.25)$$

Here, the eigenvalues ϵ_i are Kohn-Sham energies.

In Kohn-Sham equations all potential terms depends on density, therefore it needs to be solve self-consistently.

2.1.7 van der Waals Corrections

In physical chemistry, van der Waals (vdW) includes; two permanent dipoles, a permanent and a induced dipole and two instantaneously induced dipoles (London dispersion force). [37] [38] All these forces should taken into account; including covalent bonds, hydrogen bonds, electrostatic interaction because they are all important in materials [44]. In DFT, the vdW interactions are present. [39] However, a proper inclusion of vdW interactions should include the long-ranged and medium-ranged vdW interactions. The exchange-correlation functional that described in Section 2.1.5 includes vdW interaction and often approximated with LDA and GGA so that DFT is succesfull in many applications. However, LDA and GGA neglects the long-range, nonlocal vdW forces.

While studying atoms, molecules and surfaces with analysis of their polarizabilities, there is a R^{-6} (which R is the distance between two molecules or atoms) form of the London for atomic and molecular dimers, z^{-3} (z is the separation between molecular or atomic dimers) Lennard-Jones law for a neutral molecule on a surface and d^{-2} (d is the distance between molecule and surface) interaction law for pairs of solids [18] [44]. In DFT, properly representation of vdW-forces includes approximation for exhchange correlation energy in terms of the electronic density, $E_{xc}[n]$. Besides, DFT already takes into account the non-dispersive portions of the vdW interaction. However, there are many methods to include vdW dispersion correction. In Fig. 2.1 there is an overview and classifications of methods.

The vdW-DF and related methods are nonempirical ways to compute dipersion energy. In all vdW-DF schemes, the approximation

$$E_{xc} = E_x^{LDA/GDA} + E_c^{LDA/GDA} + E_c^{NL} \quad (2.26)$$

is implemented. Here, LDA and GGA is used for the short-ranged interactions and E_c^{NL} includes the dispersion energy.

There are also DFT-D methods that are semilocal corrections. They includes LDA-based approximations for short-range interactions and atom pair additive treatment of

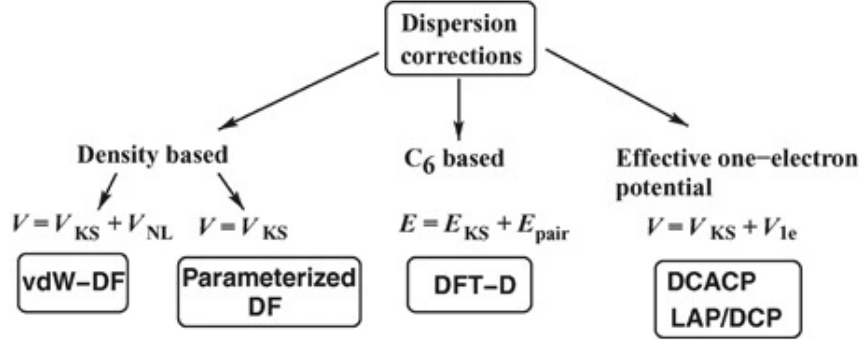


Figure 2.1: Overview of dispersion correction in DFT. E_{KS} and V_{KS} correspond to Kohn-Sham total energies and potentials. Reprinted from [47]

the dispersion energy [48].

2.2 Molecular Dynamics (MD)

Molecular Dynamics (MD) is a simulation technique where atomic trajectories of a N particle system are rather accurately created by the integration of Newton's motion equation with a particular interatomic potential. A system of particles which is governed by :

$$m_i \frac{d\vec{r}_i}{dt} = \vec{f}_i \quad (2.27)$$

where m_i is the mass of the i^{th} particle, \vec{f}_i is the force on the i^{th} particle and \vec{r}_i represents its position. The force on the i^{th} particle can be determined by taking derivative of potential as :

$$\vec{f}_i = -\frac{\partial U(r_1, r_2, \dots, r_N)}{\partial r_i}. \quad (2.28)$$

After specifying the potential energy function, the force \vec{f}_i is calculated and using this force, positions are updated in each time step in the simulation. There are several numerical schemes for solving this second order differential equation. These are based on finite difference methods and integration algorithms.

In the typical Molecular dynamic simulation, firstly system is initialized by defining the particles positions and velocities and the time step δt . Secondly, forces on ev-

ery atom is computed and Newton equations of motion is integrated using a suitable integratio scheme. Finally, again forces on every atom is computed.

The most commonly used integration algorithms are the Verlet and Velocity Verlet algorithms which will be discussed in the following sections. We performed our simulations using LAMMPS (Large-scale Atomic/Molecular/Massively Parallel Simulator) which is an open source code under GNU Public License distiributed freely by Sandia National Laboratories. [14]

2.2.1 The MD Technical issues

Each particle interacts with all of its neighbors so that the potential energy of the system varies. Therefore, determining the positions and velocities of atoms requires the solutions of the equations of motion which were mentioned in earlier. The choice for integrating the Newtons algoritm is essential such that a good algorithm should allow use of a long time step because the longer time step means fewer evaluations of the forces [64]. The most commonly used integration algorithms will be discussed in next.

In MD simulations physical quantities are calculated from time averages along the trajectories. MD simulations are performed until the properties of the system comes to an equilibration that means the properties of system doesnot change with time. In order to measure an observable, it should e express as a function of positions and momenta of the particles in the system. For example, temperature in a simulation can be defined as follow

$$\langle \frac{1}{2}mv_{\alpha}^2 \rangle = \frac{1}{2}k_B T. \quad (2.29)$$

2.2.1.1 Verlet Algorithm

Verlet integration algorithm [65] relies on Taylor expansion about t :

$$\vec{r}_i(t + \delta t) = \vec{r}_i(t) + \delta t \vec{v}_i(t) + \frac{1}{2}(\delta t)^2 \vec{a}_i(t). \quad (2.30)$$

$$\vec{r}_i(t - \delta t) = \vec{r}_i(t) - \delta t \vec{v}_i(t) + \frac{1}{2}(\delta t)^2 \vec{a}_i(t). \quad (2.31)$$

where $\vec{v}_i(t) = \frac{d\vec{r}_i(t)}{dt}$, $\vec{a}_i(t) = \frac{d\vec{v}_i(t)}{dt}$ and δt is the time step which the system propagate forward.

Using Eq. (2.30) and Eq. (2.31), the trajectories of the atoms can be iterated as

$$\boxed{\vec{r}_i(t + \delta t) = 2\vec{r}_i(t) - \vec{r}_i(t - \delta t) + (\delta t)^2 \vec{a}_i(t) + O(\delta^4)}. \quad (2.32)$$

Computing of velocities requires additional calculation in verlet algorithm and they are written as

$$\vec{v}(t) = \left(\frac{1}{2\delta t}\right)[\vec{r}_i(t + \delta t) - \vec{r}_i(t - \delta t)] + O(\delta^3). \quad (2.33)$$

The error is in the order of δ^4 and velocities and quantities depending on the velocities in the order of δ^3 so it has high accuracy. However, it requires to store two sets of positions, $r(t)$ and $r(t - \delta t)$ which requires more memory.

2.2.1.2 Velocity Verlet Algorithm

Velocity verlet algorithm is better alternative scheme and its a reformulation of verlet algorithm by manipulating expansions. It updates positions and velocities are simultaneously as

$$\vec{r}_i(\delta t) = \vec{r}_i(t) + \vec{v}_i(t)\delta t + \frac{f(t)}{2m}(\delta t)^2 \quad (2.34)$$

and

$$\vec{v}_i(\delta t) = \vec{v}_i(t) + \vec{v}_i(t)\delta t + \frac{f(t + \delta t) + f(t)}{2m}(\delta t). \quad (2.35)$$

Generally, forces on each atoms is computed using force field while $r(t)$ and $v(t)$ is given at time t . Afterwards, positions are updated as given in Eq. (2.34) and velocities are updated based on current forces. At time $(t + \delta t)$ new forces are calculated using new positions $r(t + \delta t)$ and iteration goes back to the begininig.

One of the important difference between the Verlet and Velocity Verlet algorithm is that Velocity verlet algorithm requires less memory during simulation and it is more efficient.

2.2.2 Interatomic Potentials

Interatomic potentials determines the all physical properties of a system. Interatomic potential can be written as a multibody expansion of a N atoms in a system

$$U(\vec{r}_1, \vec{r}_2, \dots, \vec{r}_N) = \sum_i U_1(\vec{r}_i) + \sum_i \sum_{j>i} U_2(\vec{r}_i, \vec{r}_j) + \sum_i \sum_{j>i} \sum_{k>j} U_3(\vec{r}_i, \vec{r}_j, \vec{r}_k) + \dots \quad (2.36)$$

where U_1 is the one-body term, U_2 is the two-body-term, U_3 is the three body term, \vec{r}_i is the position of the atom i and i, j, k run through atoms positions.

LAMMPS includes a variety of ineratomic potentials such as Tersoff-Brenner [21], Tersoff potential [23], Adaptive Intermolecular Reactive Empirical Bond Order [22] and Reactive Force Filed(ReaxFF)[24] . The Lennard Jones potential is used in order to describe van der Waals interactions and interaction between nanomaterials based on graphene. Nevertheless, there is no classical function to describe interaction for all

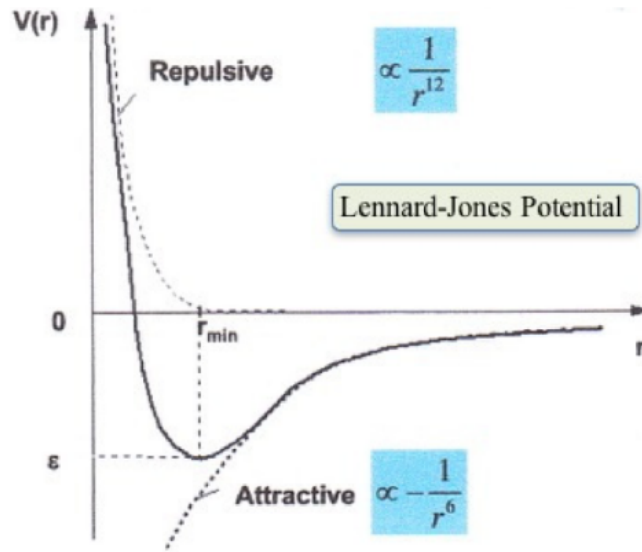


Figure 2.2: Lennard-Jones potential function. Reprinted from [13]

types material. The three most well-liked potentials for carbon materials are discussed further sections.

2.2.2.1 Lennard-Jones Potential

The Lennard-Jones potential very closely approximates interaction in noble gases whose interactions are dominated by van der Waals forces. The potential of Lennard-Jones also played a central role in the development of molecular dynamics methods, and was widely used to investigate fundamental issues such as phase transitions. Lennard-Jones potential is defined as

$$V(r) = 4\epsilon \left[\left(\frac{\sigma}{r} \right)^{12} - \left(\frac{\sigma}{r} \right)^6 \right]. \quad (2.37)$$

The potential has short-term repulsive term and long-term attractive term. The cause of the attractive force is quantum-mechanical, and linked to fluctuating dipole interactions (van der Waals) and the cause of short-term repulsive term is the Pauli repulsion. For each element, the parameters σ and ϵ are related to bond length and bond energy respectively, and are taken from experimental results.

In Fig. 2.2 potential energy graph of Lennard-Jones is shown and in the graph r_{min}

is the equilibrium distance between two atoms. Carbon atoms in the graphene are bounded to each other covalently because of this Lennard-Jones potential is not a good choice to describe the interaction of graphene.

2.2.2.2 Adaptive Reactive Intermolecular Bond Order (AIREBO) Potential

Brenner potential [21] is the principal component of the AIREBO potential [22], while some extra functions are added to it. The covalent interaction describing part is remain unchanged in the AIREBO potential and additional functionals describe the short range. For carbon based systems, AIREBO was used to model the mechanical properties successfully [25].

In AIREBO the interatomic interaction is given by [26]

$$E_b = \sum_i \sum_{j(j>i)} [V_R(r_{ij}) - B_{ij}V_A(r_{ij})]. \quad (2.38)$$

where r_{ij} is the distance between atoms i and j , B_{ij} is an empirical function and V_R and V_A is repulsive and attractive parts functions. In the REBO potential dispersive and intermolecular interactions such as short repulsion does not included. In AIREBO potential dispersive and intermolecular interactions are described by the Lennard-Jones potential which described in above. Also, the original REBO potential excludes the rotational interaction because of this another additional part is defined in AIREBO potential that depends on angles between bonds. Resultantly, the total energy for AIREBO potential can be written as

$$E = E_{REBO} + E_{LJ} + E_{Tors}. \quad (2.39)$$

where E_{REBO} is the energy calculated from the AIREBO potential. E_{LJ} is calculated from LJ potential and E_{Tors} is calculated from potential for rotation of the system. Usage of AIREBO potential in LAMMPS as follow:

```
Usage of AIREBO potential in LAMMPS
pair style airebo 3.0
pair coeff CH. airebo C path, name, element
```

2.2.2.3 Reactive Force Field (ReaxFF)

Although the potentials we mentioned were designed to describe the carbon carbon interactions, they are insufficient in carbon-based nanomaterials, including atoms other than carbon such as hydrogen, oxygen and nitrogen. In the non-reactive potentials, bonds can be stretched or twisted in interactions. However, they can not be broken such that chemical reactions can not be simulated. The developed ReaxFF potentials include additional terms in order to modify bond strength depending on environment so that bonds can be broken and re-formed and they include nonbonded forces such as van der Waals. Therefore, in MD simulations ReaxFF [15] is used.

The ReaxFF energy terms are given as [26]

$$E_{system} = E_{bond} + E_{over} + E_{under} + E_{lp} + E_{val} + E_{tor} + E_{vdW} + E_{Coulomb}. \quad (2.40)$$

where E_{bond} is the valence bond energy, E_{over} and E_{under} is the over and under coordination energy penalty, E_{lp} is the lone pair energy, E_{val} is the valence angles energy, E_{tor} is the torsion angles energy, E_{vdW} is the van der Waals energy and $E_{Coulomb}$ is the Coulomb interaction energy.

There are different versions of reaxFF such as *ReaxFF_{CHO}*[24], *ReaxFF_{C2013}* [27] and *ReaxFF_{LG}* [28]. In our simulations, we used *ReaxFF_{LG}*. Usage of *ReaxFF_{LG}* potential in LAMMPS as follow:

```
Usage of the ReaxFF LG in LAMMPS
pair style reax/c lmp control
pair coeffffield.reax.lg C H O
```

2.2.3 Thermodynamical Ensembles

2.2.3.1 Microcanonical (NVE) Ensemble

Since MD uses Newton equations of motion in order to simulate kinetic and thermodynamic properties of a molecular system and all forces in Newton equation of

motions are related to the potential energy of the system, then total energy of the system is conserved. If total volume(V) and number of atoms(N) are also kept constant, then simulation is performed in the microcanonical (NVE) ensemble. For a system of N molecules that move with time in NVE ensemble, the total number of particles N, total energy E and total volume does not change with time. The periodic boundary conditions is applied in order to kept the volume of simulation constant. In large NVE systems the temperature variations are small and roughly constant. Some situations require a constant temperature. Thus, MD must reproduce an isothermal ensemble such as canonical NVT, in which the number of particles, volume and temperature are kept constant.

2.2.3.2 Canonical (NVT) Ensemble

In a canonical ensemble, number of atoms(N), volume(V) and temperature(T) of the system is conserved. Maintaining a constant temperature means the system in a thermal interaction with a heat bath. From Maxwell-Boltzmann distribution, the relationship between the target temperature T and the kinetic energy of a system can be wirtten as follow:

$$k_B T = m \langle v_\alpha^2 \rangle \quad (2.41)$$

here m is the mass of the particle and v_α is the α th component of the system. This relationship is often used in MD simulation in order to measure the temperature [63]. In MD simulations, constant temperature is achieved by thermostats such as deterministic thermostats; Nosé-Hoover [51] and stochastic thermostats; Langevin thermostat [52].

2.2.3.3 Isothermal-Isobaric Ensemble

If the system has fixed number of atoms (N) and temperature(T) so it is istohermal. Also, fixing the pressure (P), makes the system isobaric. In MD simulation, volume changes with time during the simulation.

2.2.4 Temperature Control in MD Simulations

2.2.4.1 Velocity rescaling

The best way to control temperature is based on the velocity rescaling. From the Maxwell-Boltzmann (MB) distribution, one can obtain the average kinetic energy per degree of freedom is related to temperature as

$$\left\langle \frac{mv_{i,r}^2}{2} \right\rangle = \frac{1}{2}k_B T. \quad (2.42)$$

where $r = (x, y, z)$ components of the i^{th} atom. Here brackets represent the ensemble average and it corresponds to the average velocities of all atoms. Therefore instantaneous temperature $T(t)$ can be written as

$$k_B T(t) = \frac{1}{N_f} \sum_{i,r} mv_{i,r}^2. \quad (2.43)$$

where N_f is the number of degrees of freedom. $T(t)$ does not correspond to T that is used to generate MB distribution. In order to keep temperature constant ($T(t)=T$), one can rescale the velocities as

$$v_{i,r} = \sqrt{\frac{T}{T(t)}} v_{i,r}. \quad (2.44)$$

However, even in the canonical system instantaneous temperature fluctuates and the canonical ensemble disturbed by its fixing. There are different methods to control the temperature such as weak coupling with heat bath that was proposed by Berendsen [29], stochastic coupling that was proposed by Andersen [30] and Nose-Hoover method [31].

2.2.4.2 Berendsen Thermostat

Berendsen thermostat [29], either removes or adds energy to the system to maintain constant temperature. The velocities are scaled at each step, so that the temperature

change is determined by

$$\frac{dT}{dt} = \frac{1}{\tau}(T_{target} - T). \quad (2.45)$$

where T_{target} is the target temperature and τ is the coupling constant. The velocities rescale as

$$v'_{i,r} = \lambda v_{i,r}. \quad (2.46)$$

where $\lambda^2 = 1 + \frac{\Delta t}{\tau} \left(\frac{T_0}{T} - 1 \right)$.

Usage of Berendsen thermostat in LAMMPS is given as:

```
Usage of Berendsen thermostat in LAMMPS
fix ID group ID temp/berendsen Tstart Tstop Tdamp
fix 1 all temp/berendsen 300.0 300.0 100.0
```

2.2.5 Molecular Dynamics using LAMMPS

LAMMPS can run on a single processor or in parallel, and thus can run multiple simulations from a single input script simultaneously. The input script contains syntax to define and use variables and formulas, as well as to loop over runs and break loops. It also consists of commands for defining and generating geometry, types of atoms, boundary conditions, fields of force and other parameters for simulation control. Thermodynamic information and text files which can be customized at the end of the simulations. Also required data is given as output.

2.2.5.1 The structure of a typical LAMMPS input

In LAMMPS, the simulation starts by reading an input file. It reads one row in the file at a time and executes the commands and acts accordingly. Hence, both positional order and command structure are important.

In the first part of the script, there are parameters that need to be firstly defined such as dimensions, atom style, boundary and units. In LAMMPS, all interatomic potentials is used in different unit sytems. Therefore, choosing the suitable time step is important. For example, AIREBO potentials work in metal units while ReaxFF works in real units which described as below.

metal units:

- time = picoseconds
- distance = Angstrom
- temperature= Kelvin
- energy = eV
- pressure = bars
- mass = grams/mole

real units:

- time = femtoseconds
- distance = Angstrom
- temperature= Kelvin
- energy =Kcal/mole
- pressure = atmospheres
- mass = grams/mole

Settings which govern the simulation are specified after defining the prerequisites and creating atoms and geometries. One of the most important is force field that used to calculate potential function of pairs of bonded atoms.

Specifying the inital temperature of the simulation, set the inital velocities of atoms with a specified distribution. In LAMMPS, the velocities in simulation are generated using velocity command and its usage as follow:

```
Usage of velocity command in LAMMPS
velocity group ID style args keyword value ...
velocity all create 300.0 4928459 rot yes dist gaussian
```

Here the create style generates an ensemble of velocities using random number generator with specified seed at target temperature [66]

Controlling operations such as velocity control, position updating, applying force, temperature control are reached by fix command. Positions and velocities are updated through constant integration of NVE, NPT, and NVT time. Properties such as kinetic energy, potential energy, temperature and pressure can be obtained from the simulations for a group of atom.

CHAPTER 3

RESULTS AND DISCUSSION

In this thesis, We studied the interface properties between graphene and PEEK by starting with density functional theory (DFT) in order to study the quantum mechanical roots of the interaction. For larger system we used the molecular dynamics framework within the reactive force-field (ReaxFF).

In our calculations the adsorption energies were calculated using

$$E_{ads} = E_{System} - E_{Graphene} - E_{Molecule} \quad (3.1)$$

where E_{ads} is the adsorption energy, E_{System} is the energy of the system and $E_{Graphene}$ and $E_{Molecule}$ is the energy of the graphene and molecule.

3.1 DFT Results

3.1.1 Benchmark Calculations

In order to gain some confidence in the simulation procedure and the results obtained from Quantum Espresso, we benchmarked the graphene lattice constant calculation. During the benchmarking, three different van der Waals schemes, DFT-D, vdW-DF and vdW-DF-C09 [43] were used to calculate the lattice constant of graphene with a PBE(Perdew-Burke-Ernzerhof) exchange-correlation. The energy cutoff was 40 Rydberg and 1x1x10 k-point mesh was used. A 2x2 graphene sheet was constructed using a series of C-C bonds in a range from 1.38 to 1.44 Å and by using a third order polynomial fit, the lattice constant for graphene is obtained. The values for the

graphene lattice constant with three methods and the graphs used in the fits are shown in Table 3.1 and in Fig. 3.1

Table 3.1: Graphene lattice constant with DFT-D, DFT-DF and DFT-DF-C09

Methods	DFT-D	DFT-DF	DFT-DF-C09
Lattice constants (\AA)	1.422	1.423	1.420

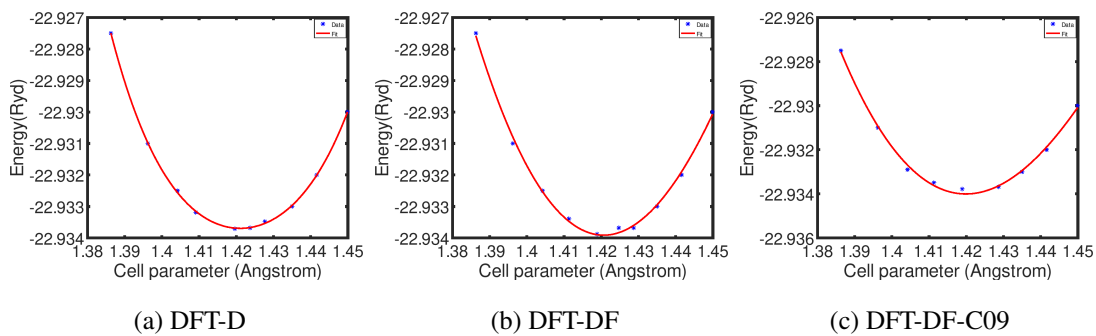


Figure 3.1: Graphene lattice constant

As seen in these results, vdW-DF with exchange of Cooper (vdW-DF-C09) gives the most accurate result for lattice constant of graphene since its experimental value is 1.42 \AA [53]. Therefore, this functional is used in our DFT studies.

Next, we focused on the interaction of PEEK and its sub-units on graphene substrate within DFT. In all calculations, 11 \AA vacuum distance was added to avoid periodic interaction between periodic images and the kinetic energy cut-off was set to be 30 Ryd. In the adsorption energy calculations, a 3x3x1 k-point mesh is used for Brillouin zone integrations.

3.1.2 Graphene-PEEK

We begin by dividing the PEEK monomer into three sub-units, and studying each sub-unit's interaction with the graphene separately. In Fig. 3.2 the three subunits of PEEK is shown.

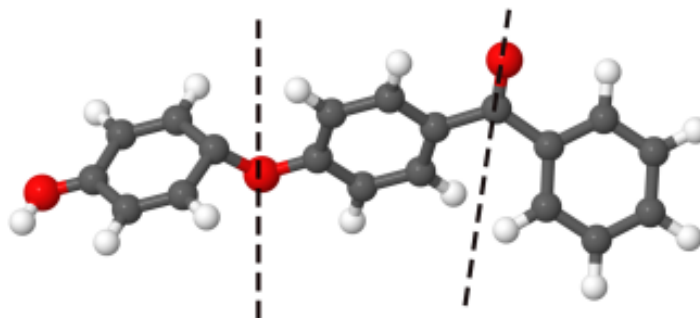


Figure 3.2: Sub-units of PEEK. The carbons are gray, the hydrogens are white, and the oxygens are red.

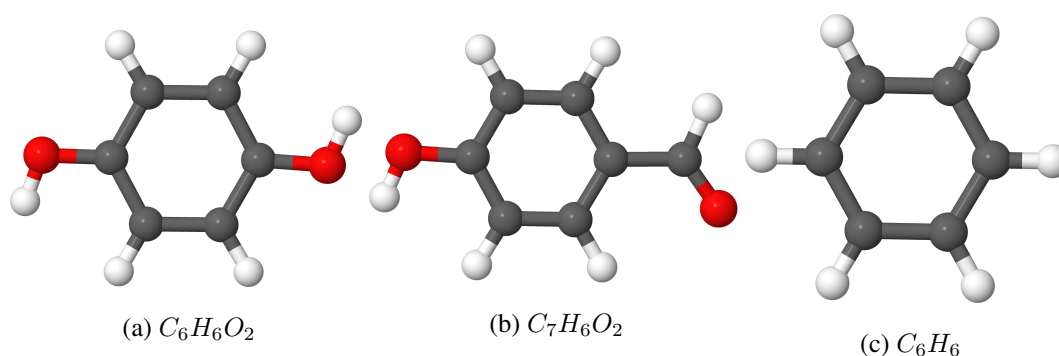


Figure 3.3: Sub-units of PEEK as used in our calculations; $C_6H_6O_2$, $C_7H_6O_2$ and C_6H_6

The rings in Fig. 3.3 was placed 3\AA above the 6×6 graphene sheet and rotated 30° , 60° and 90° in order to investigate different configurations as shown by Fig. 3.4 and adsorption energies were calculated using Eq. (3.1). The adsorption energies and average distances are given in the Table 3.2. The distances given in the Table 3.2 are the average distances calculated from the carbon atoms just below the middle of the aromatic ring to each atom in the molecule.

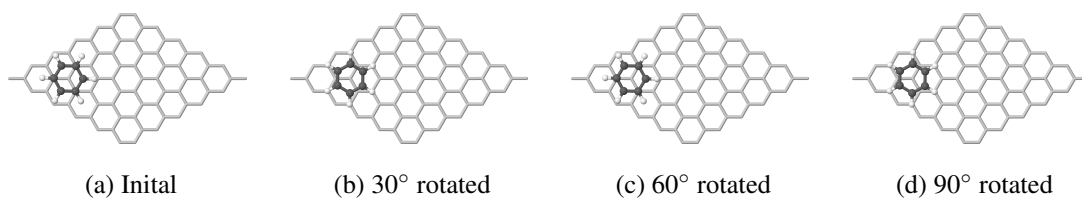
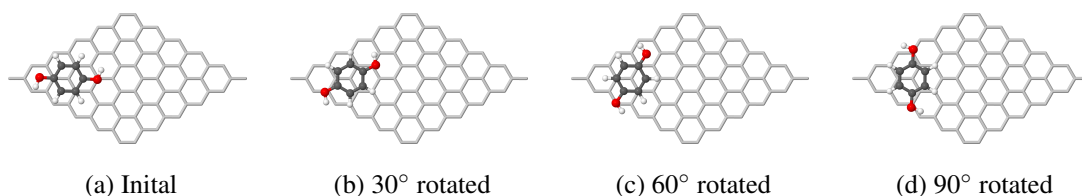


Figure 3.4: Different configurations of C_6H_6

For the benzene ring, because of the symmetry, 0° and 60° has the same geometry and almost same adsorption energy. The same conclusion can also be reached for configurations of 30° and 90° .



In the case of $C_6H_6O_2$, the original 0° has the highest adsorption energy and due to the existence of oxygen atoms, adsorption energies are higher than benzene rings.

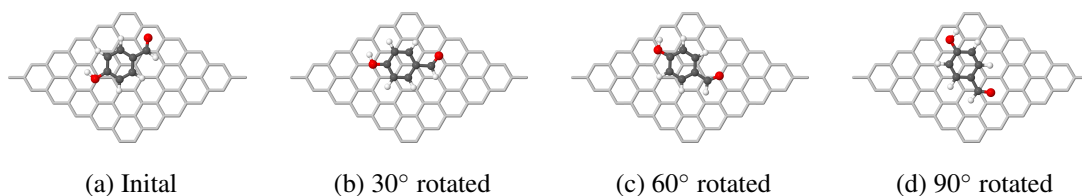


Figure 3.6: Different configurations of $C_7H_6O_2$

Finally, adsorption energies of $C_7H_6O_2$ sub-units on graphene as shown in Fig. 3.6 were calculated. The orientation with 90° has the higher adsorption energy in all three sub-units because of the oxygen atoms and atom number. The results are given in Table 3.2. As expected the adsorption energy, due entirely to the van der Waals interaction, grows with growing size of the molecule. The molecule which contain oxygen rest slightly closer to the graphene sheet, which again is expected due to the larger polarizability of these molecules.

Table 3.2: Adsorption energies (eV/molecule) and adsorption distances (Å) of $C_7H_6O_2$, $C_6H_6O_2$ and C_6H_6 subunits on graphene. The values in boldface indicate the most stable orientations for each subunit.

	Gr+C ₇ H ₆ O ₂		Gr+C ₆ H ₆ O ₂		Gr+C ₆ H ₆	
	E_{ads}	d	E_{ads}	d	E_{ads}	d
0°	-0.848	3.27	-0.778	3.23	-0.617	3.28
30°	-0.830	3.28	-0.770	3.25	-0.613	3.29
60°	-0.837	3.27	-0.778	3.24	-0.617	3.28
90°	-0.863	3.24	-0.769	3.24	-0.613	3.29

Following the sub-unit calculation, the PEEK monomer was placed on a 8x8 graphene as shown in Fig. 3.7. The initial of the PEEK monomer were taken from an MD simulation at 10K with a duration 1ns. As in the sub-unit's adsorption energy calculations, geometry optimization is performed. The energy of PEEK is calculated in a large simulation box and a single step self-consistent calculation is performed so that the contribution due to distortion of the molecule is eliminated.

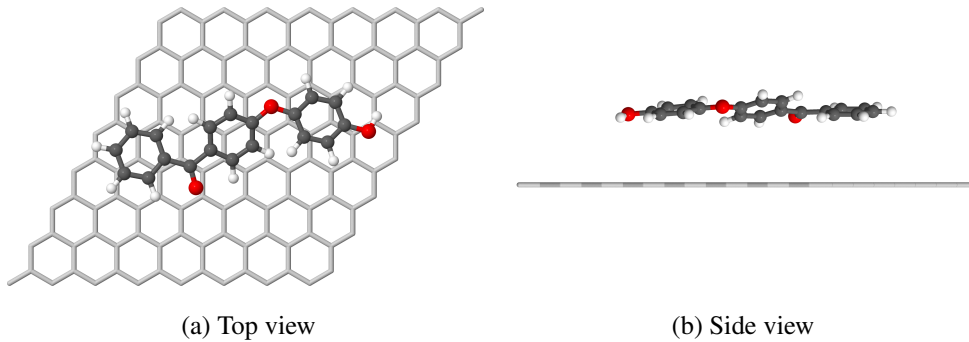


Figure 3.7: PEEK monomer on graphene

The adsorption energy of the PEEK molecule as seen in Fig. 3.7 was calculated to be -0.141 eV. This adsorption energy is clearly lower than what would be expected from a simple addition of the parts of the molecule, even when corrected by the extra atoms added for the calculations. This outcome can be explained by the fact that unlike

the individual molecules, the aromatic rings in the monomer do not necessarily align perfectly with the graphene substrate but can rotate to accommodate the H-H repulsion. The relative angles of the aromatic rings will be seen to play an important role in the determination of adsorption energies.

3.2 MD Results

3.2.1 Benchmark Calculations

Similarly to the DFT calculations, we benchmarked the graphene lattice constant calculation also at the beginning of the MD part of our calculations. The lattice constant for graphene is obtained as 1.40 Å as shown in the graph Fig. 3.8.

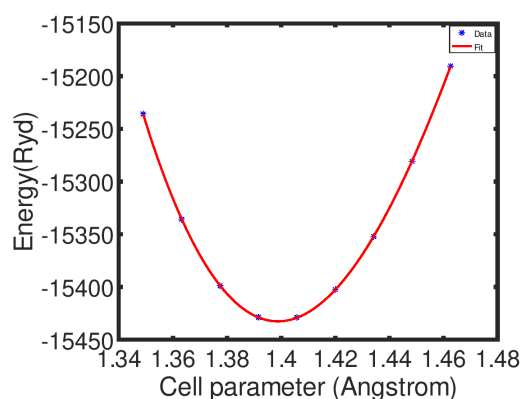


Figure 3.8: Graphene lattice constant using AIREBO

All MD calculations were performed using LAMMPS an open source code under GNU Public License called distributed freely by Sandia National Laboratories [20]. We used ReaxFF_{LG} potential in our simulations.

3.2.2 Graphene-PEEK monomer

As a further check of our MD protocol, we repeated the sub-unit calculations at 0K, 100K and 300K. In the calculations at 0K, after minimization of the system, the final configurations of the constituent parts, namely graphene and the adsorbate of the

composite system, were separated and their static energies were taken at the final stage and the adsorption energy was calculated using the Eq. (3.1).

Following the static calculations, graphene-PEEK sub-units and graphene-monomer adsorption energy calculations were performed in the NVT ensemble. The graphene substrate was kept immobile and fixed in space during the calculations. This is a popular practice in similar simulations in the literature. Periodic boundary conditions were applied in all dimensions. All equations of motion were integrated by using the velocity Verlet algorithm and the Berendsen thermostat is used to achieve a constant temperature with a damping factor of 100 which means that the thermostat is activated every 10 fs during the simulation. The temperature vs time graph at 100K and 300K are given in Fig. 3.11a and Fig. 3.11b. Potential energy of the system is averaged using the last 50 ps of the simulation and potential energies of graphene and polymer are taken from the last step of the simulation. The adsorption energies (in meV) of sub-units and PEEK monomer on 6x6 graphene sheet with different temperatures and DFT adsorption energies are given in the Table 3.3

Table 3.3: Adsorption energies (in eV) of sub-molecules on 6x6 graphene

System	DFT	ReaxFF		
		T=0K	T=100K	T=300K
GR/C ₆ H ₆	-0.617	-0.754	-0.765	-0.754
GR/C ₇ H ₆ O ₂	-0.848	-0.872	-0.862	-0.778
GR/C ₆ H ₆ O ₂	-0.778	-0.793	-0.809	-0.736
GR/PEEK Monomer	-0.141	-0.127	-0.880	-0.700

The ReaxFF calculation at T=0K are in overall good agreement with DFT results both for the sub-units and the monomer.

While adsorption energies decrease with increasing temperature, different configurations of PEEK monomer on the top of graphene is observed as shown in Fig. 3.9.

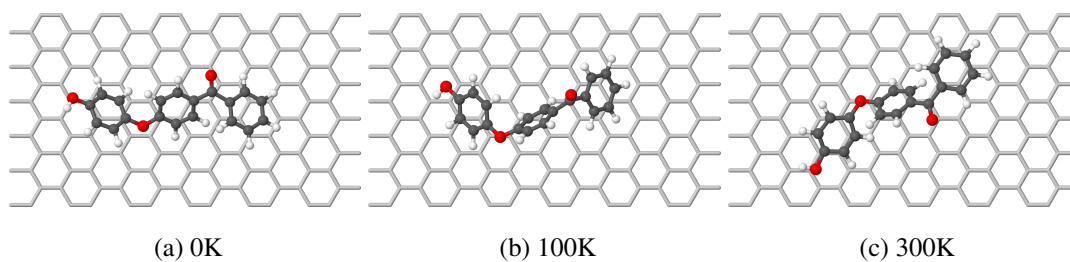


Figure 3.9: Final configurations front view of PEEK monomer on graphene at (a) 0K, (b) 100K and (c)300K

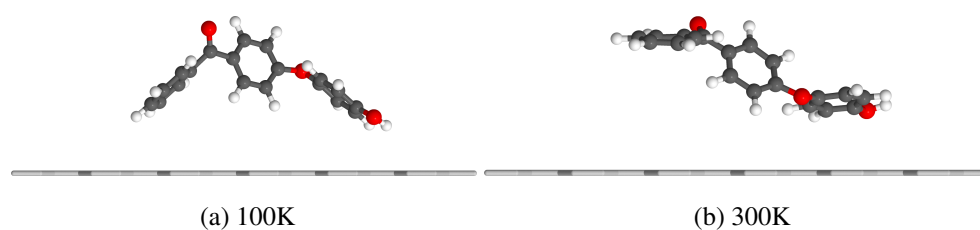
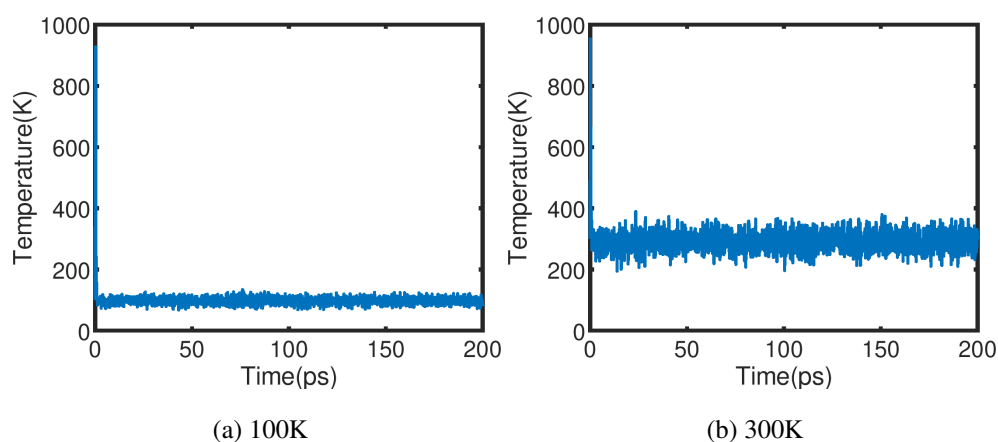


Figure 3.10: Final configurations side view of PEEK monomer at (a) 100K and (b) 300K

As one can see Fig. 3.10a the first and last rings are tilted. On the other hand in Fig. 3.10b, the last ring of PEEK monomer tends to more align with the graphene sheet while the other rings are tilted this can cause a decrease in interaction energy due to a larger distance between PEEK monomer and graphene.



3.2.3 Graphene and PEEK chains

After comparing DFT and MD results for graphene/PEEK sub-units and monomer adsorption energies, we study adsorption energies of longer chains of PEEK polymer. We calculate the interaction energies of 3, 6 and 9 monomer PEEK chains on graphene sheets that initial position are given in Fig. 3.12a, Fig. 3.12b and Fig. 3.12c. As in the graphene-monomer interaction, these simulations were conducted at 100K, 300K and 500K. The front and side views of the final configurations of N-chain PEEK molecules are given in the Fig. 3.13, Fig. 3.14 and Fig. 3.15

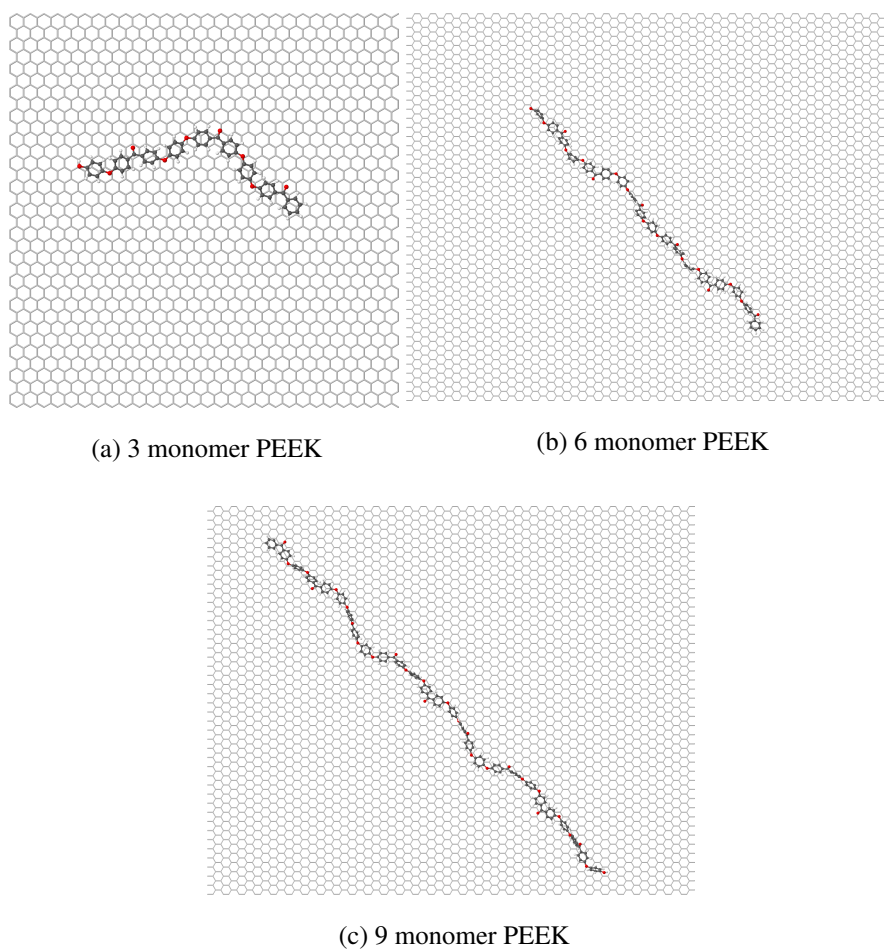


Figure 3.12: Initial configurations front view of (a) 3 PEEK, (b) 6 PEEK and (c) 9 PEEK on graphene

In the calculation of adsorption energies we used the same protocol except that simu-

lution time is increased 200 ps to 400 ps. We calculated the adsorption energies from snapshots taken every 10 ps during the last 100ps of the simulation. Adsorption energy versus time graphs which are produced using these 10 adsorption energy results are given in the Fig. 3.16. The obtained adsorption energy result for N-chain PEEK molecules with respect to the temperature is given in the Table 3.4.

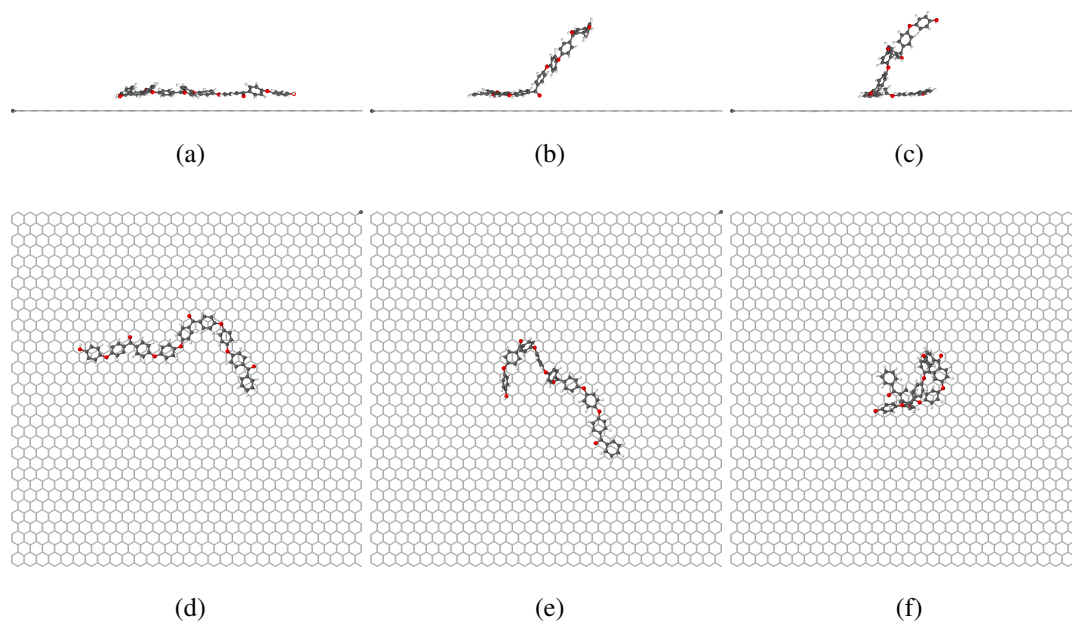


Figure 3.13: Final configurations of 3 monomer PEEK on graphene at different temperatures (a), (b), (c) side views and (d), (e), (f) are top views.

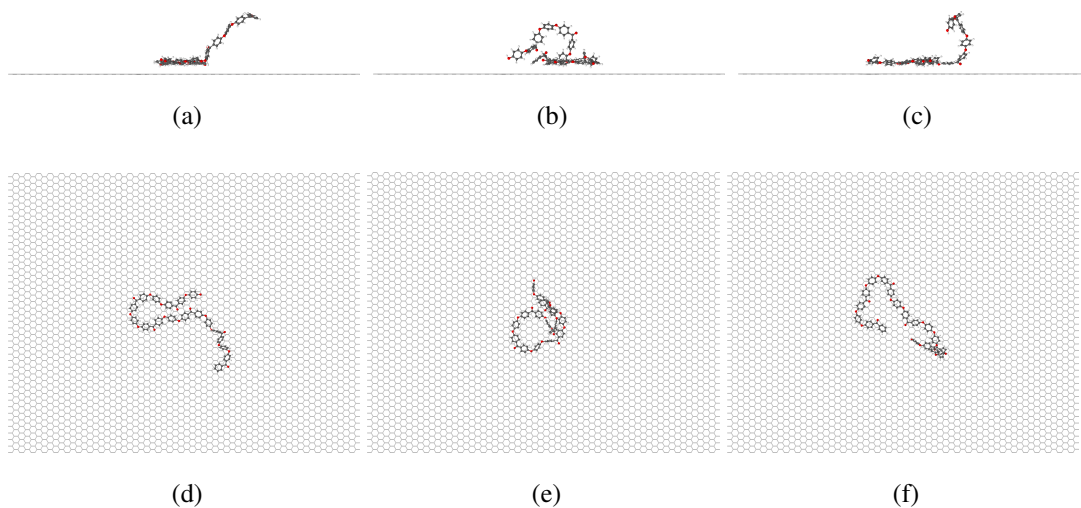


Figure 3.14: Final configurations of 6 monomer PEEK on graphene at different temperatures (a), (b), (c) side views and (d), (e), (f) are top views.

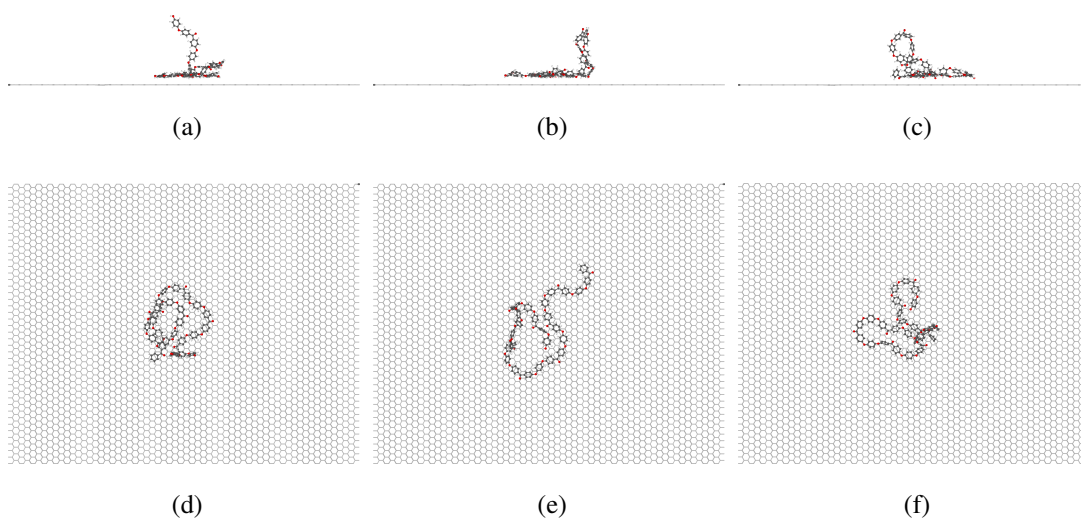


Figure 3.15: Final configurations of 9 monomer PEEK on graphene at different temperatures (a), (b), (c) side views and (d), (e), (f) are top views.

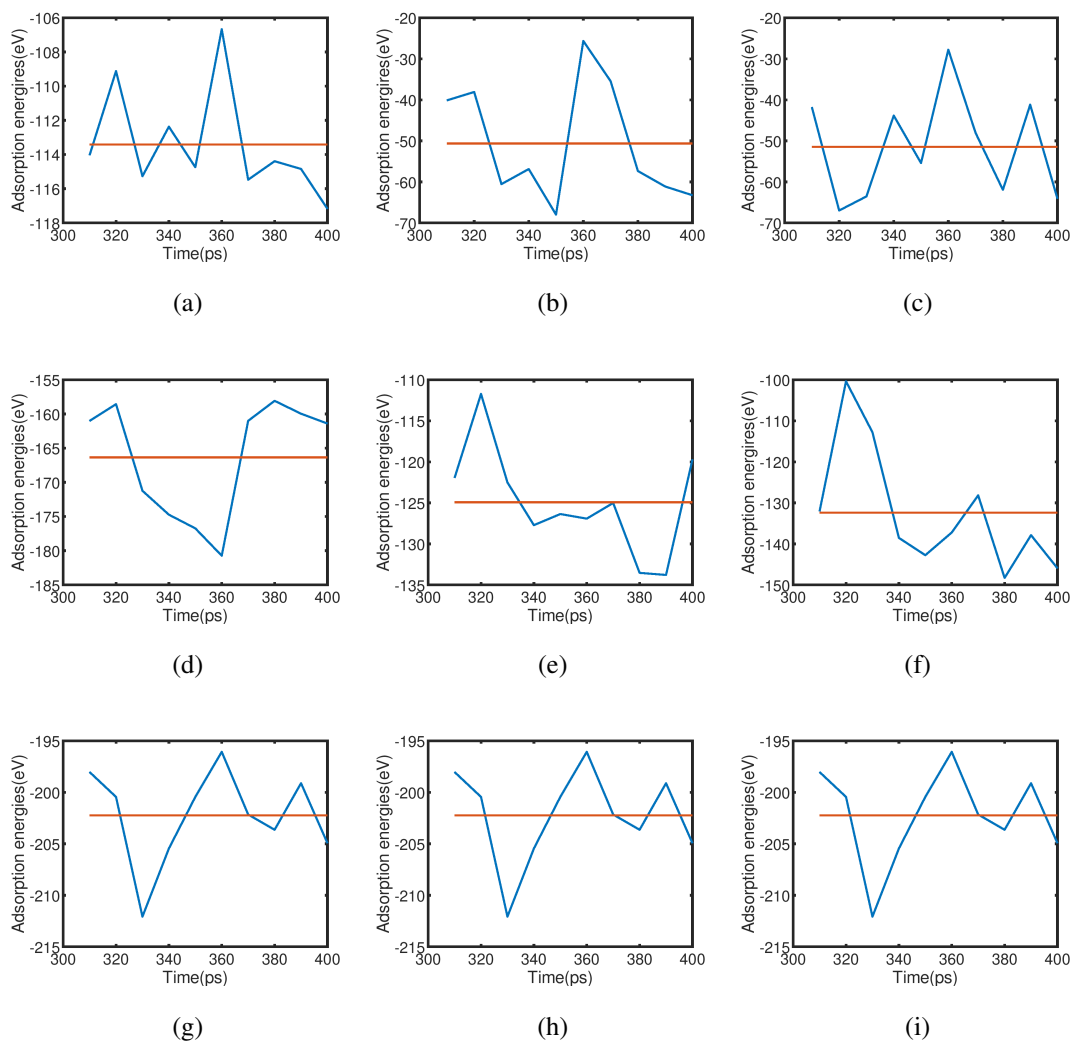


Figure 3.16: Adsorption energy graphs of 3 monomer PEEK on graphene at $T=100\text{K}$, $T=300\text{K}$ and $T=500\text{K}$. Blue lines represent the energies taken every 10 ps during the last 100 ps of the simulation and red lines are averages.

Table 3.4: Adsorption energies (in eV) of rod-like PEEK chains adsorbed on graphene as a function of temperatures

	Gr/3PEEK	Gr/6PEEK	Gr/9PEEK
100K	-4.88	-7.13	-8.70
300K	-2.18	-5.37	-9.26
500K	-2.21	-5.78	-7.80

As one can see from Table 3.4, there is a general decreasing trend in adsorption energies when temperature is increased. This is attributed to smaller number of atoms interacting which will be discussed in next. Also, the adsorption energies at 300K and 500K are similar except for 9 PEEK monomer at 300K. The reason for that 9 PEEK chain is longer and more folded at 300K.

Radius of gyration is one of the basic properties associated with polymers. It gives an understanding of polymer folding and calculated using :

$$\vec{R}_g^2 = \frac{1}{M} \sum_i (\vec{r}_i - \vec{r}_{cm})^2 \quad (3.2)$$

where M is the total mass of the atoms in the polymer chain and \vec{r}_{cm} is the center of mass position. As stated by this equation, a larger radius of gyration means that polymer is more extended whereas a smaller value means that it is folded. In our studies, the radius of gyration is investigated as a figure of merit. The radius of gyration of N-chain PEEK molecules on graphene sheet at 100K, 300K and 500K is given in Fig. 3.17.

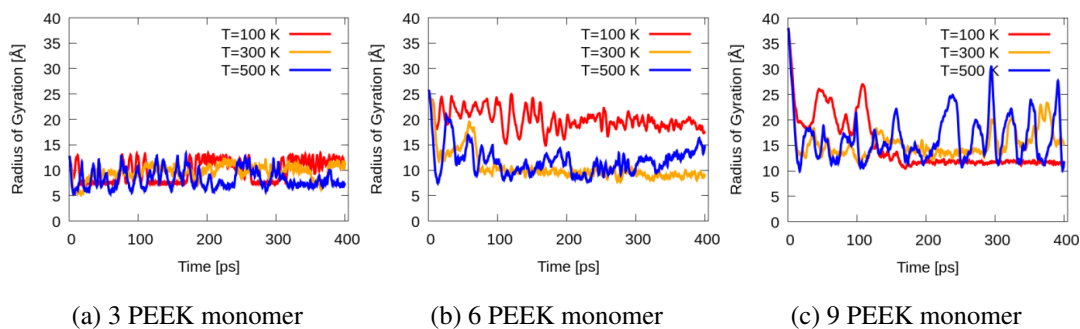


Figure 3.17: The radius of gyration of the N-chain PEEK molecules on the graphene sheet for three different temperatures (a) 3 PEEK monomer, (b) 6 PEEK monomer, (c) 9 PEEK monomer

As one can see from Fig. 3.18a, the radius of gyration is smaller for 3 PEEK monomer. In the case of 6 PEEK monomer, because of the folding of polymer chains at 300K and 500K as can be seen from Fig. 3.14, radius of gyration decreases as compared to 100K. Also, in 9 PEEK monomer calculations, there is a fluctuation in the radius of gyration at 500K because of the folding and unfolding behaviour of the polymer chains during the simulation.

Furthermore, we investigated the linear distribution of PEEK atoms on graphene as function of distance from graphene surface. The peak visible at around % 20 of atoms in all plots is attributed to the atoms aligned with the graphene. For all calculations, linear distributions are given in Fig. 3.18. From these figures, one can see that the effect of temperature decreases with increasing chain lengths since longer polymer chains are more folded.

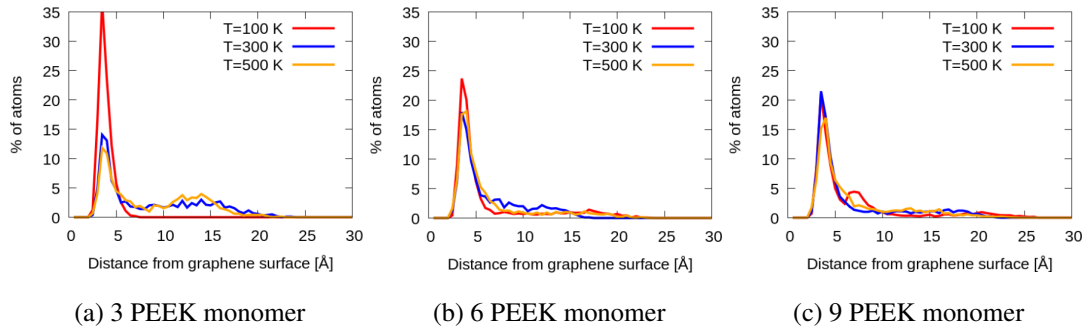


Figure 3.18: Linear distribution of N-chain PEEK molecules chains on graphene (a) 3 PEEK monomer, (b) 6 PEEK monomer, (c) 9 PEEK monomer

3.2.4 Graphene-PEEK Polymer Sliding

An understanding the physics of atomic friction has an important role a in wide range of applications. Nanotribological studies are performed by Atomic Force Microscopy (AFM) [32] or Friction Force Microscopy (FFM) [33] in order to measure normal and lateral forces. Theoretical calculations of nanotribological properties have been investigated within DFT and MD [54] [55]. While DFT calculations uncover the quantum mechanical origins of mechanisms contributing to friction, they are computationally costly and therefore can only include up to a few hundreds of atoms. On the other hand, classical MD calculations not only can handle a much larger number of atoms at a time but can also simulate temperature-dependence in longer simulations.

Tomlinson model is one of the most well-known model that is used to describe friction in microscopic scale. It is a simple one dimensional model that is introduced by Tomlinson in 1929 [72]. In the model, a particle with mass m attached via a spring of strength k . The support is sliding with a constant velocity in a potential as shown in Fig. 3.19. The stick-slip process occurs when the energy built up in the spring is enough to pull the particle across the potential barrier.

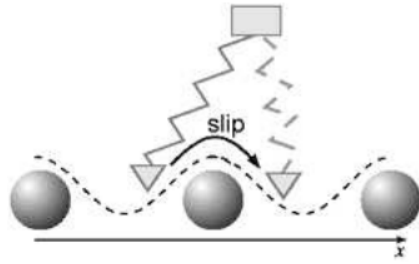


Figure 3.19: A sketch of the Tomlinson model, The dashed lines indicates the periodic potential, and the particle is sketched as a triangle. Reprinted from [73]

While sliding, if the spring energy is dominant in the trajectory of the particle, the support moves across the potential barrier uniformly. If the external potential dominant in the trajectory, then the particle stays in a potential minimum until the energy is built up in the spring is enough to pull the particle across the external potential energy barrier.

In this chapter so far, we have concentrated on the static properties of the interface between the polymer and graphene components of the system. In this subsection we concentrate on the dynamics of the same interface. We report on the adhesion characteristics between graphene and PEEK oligomers as they slide past one another as a function of such important parameters as velocity, temperature and chain length.

In all calculations, the front ring of PEEK chains are assigned as *driver* atoms and the other parts are assigned as *mobile* atoms. The driver atoms are kept rigid with respect to one another throughout the simulation and are displaced with a constant velocity. The mobile atoms on the other hand are placed under no restriction and are allowed to freely. After an initial optimization, the system temperature is kept constant during 400 ps in the NVT ensemble. Berendsen thermostat is used with a damping factor 100 which means that thermostat is activated every 10 fs during the simulation. After waiting in the NVT ensemble at different temperatures (1K, 100K and 300K) constant velocities is assigned to driver atoms during 4 ns in positive x direction. During the simulations, the graphene substrate was kept immobile and fixed in space. Forces on mobile atoms are calculated at every steps while sliding. Average friction force between graphene and PEEK chains is calculated from average

forces on mobile atoms in negative x direction.

Firstly, in order to investigate the velocity dependence of friction force on the smallest of the systems under investigation here, namely three-chain is placed on the top of the graphene sheet. The three-chain is displaced with velocities of 1 m/s, 10 m/s and 100 m/s on graphene at 1K. The forces on mobile atoms vs time graphs are given in Fig. 3.21. Also, the average friction forces on mobile atoms as a function of velocities are given Table 3.5. Average forces are calculated from time averages of forces on mobile atoms during the simulation.

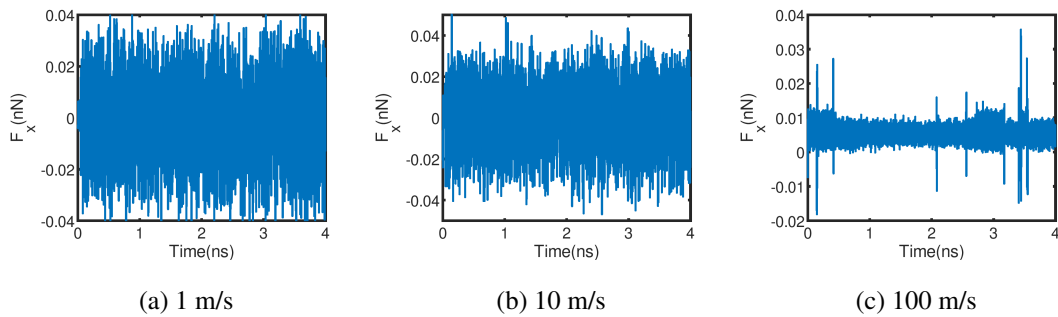


Figure 3.20: Force on mobile atoms of 3 PEEK monomer during sliding with velocities 1 m/s, 10 m/s and 100 m/s

Table 3.5: Friction force between PEEK monomer and graphene as a function of velocity

Velocity(m/s)	1	10	100
Friction force (nN)	-0.0132	-0.0130	-0.0056

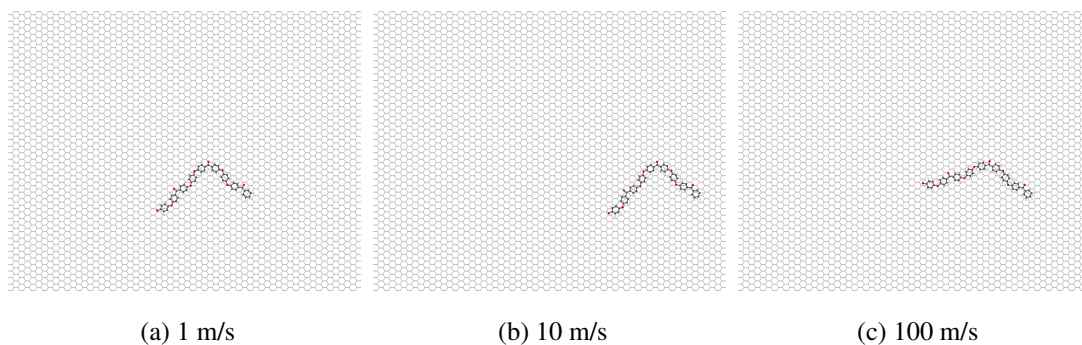


Figure 3.21: Configurations of 3 PEEK molecules sliding with velocities of 1 m/s ,10 m/s and 100 m/s

As one can see from Table 3.5 and Fig. 3.21, for 100 m/s velocity, friction force is slightly lower than friction force with velocities of 1m/s and 10 m/s. In the simulations of 100 m/s PEEK chains remained in rod-like shape whereas in 1 m/s and 10 m/s calculations, they took a v-shaped form as shown in Fig. 3.21 and experience a motion like stick slip whereas pulling the atoms with higher velocities cause a uniform motion. The left side of bending portion of PEEK molecules in Fig. 3.21a and Fig. 3.21b oscillates at low velocities, since the molecule stays in a potential minimum until the energy built up in the molecule is large enough to pull the molecule across the potential barrier. So at first, the molecule stays in the position of the minimum of potential and then it suddenly slips over the barrier into new potential minimum. However, at high velocities, molecules is pulled across the potential barrier in a uniform way. As a consequence, while sliding with velocities of 1m/s and 10 m/s friction forces are similiar and with velocity of 100 m/s, friction force is lower.

Afterwards, we investigated the effect of temperature (at 1K, 100K and 300K) and chain lengths (3-,4-,5- chains PEEK molecules).

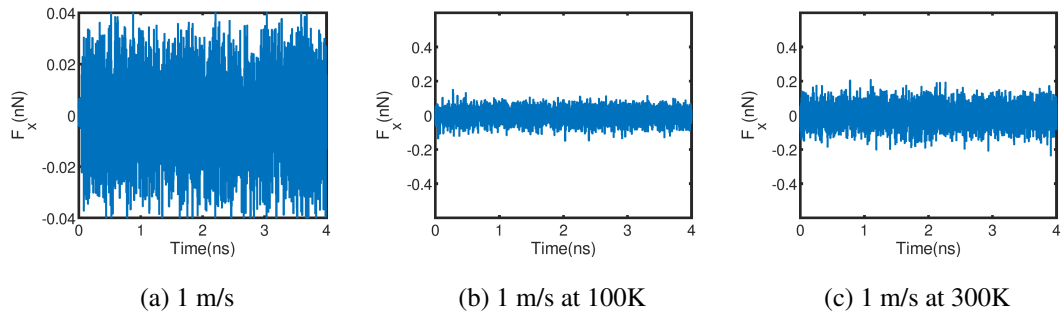


Figure 3.22: Friction force on mobile atoms of 3 PEEK during sliding with velocities of 1m/s at 100K and 300K

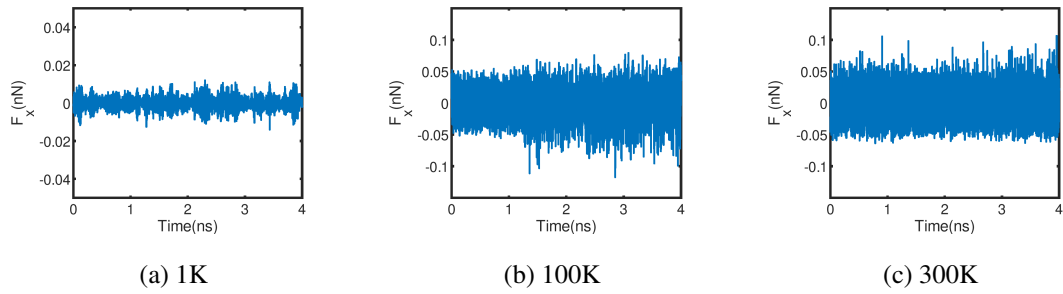


Figure 3.23: Friction force on mobile atoms of 4 PEEK sliding with a velocity of 1 m/s at 1K, 100K and 300K

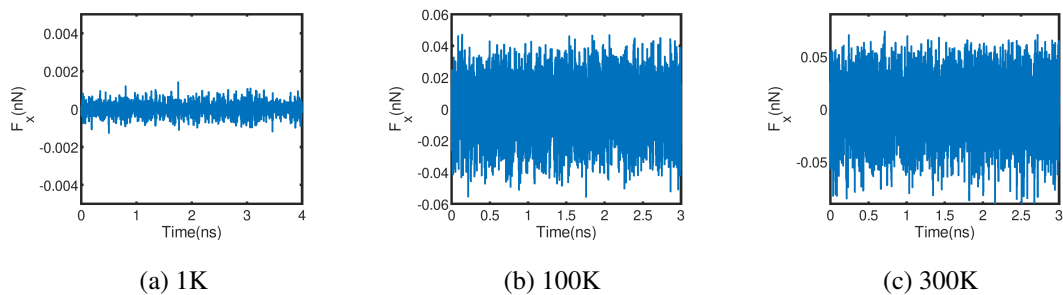


Figure 3.24: Friction force on mobile atoms of 5 PEEK sliding with a velocity of 1 m/s at 1K, 100K and 300K

Table 3.6: Friction force between graphene and N-chain PEEK molecules as a function of temperatures

	GR/3PEEK	Gr/4PEEK	Gr/5PEEK
1K	-0.0132	-0.0026	-0.0002
100K	-0.0326	-0.0238	-0.0160
300K	-0.0492	-0.0277	-0.0265

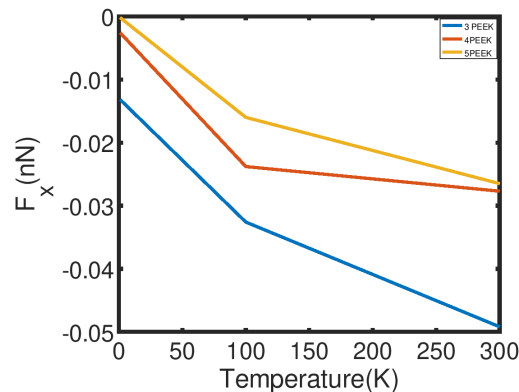


Figure 3.25: Friction forces between N-chain PEEK molecules and graphene sheet as a function of temperature

As one can see from Fig. 3.25 and Table 3.6, increasing chain length decreases the friction forces. This is because of the folding of longer peek chains. For example, at 1K calculation three-chain PEEK molecule is more aligned with the graphene sheet whereas four-chain and five-chain molecules are folded as shown in Fig. 3.26. Also, at higher temperatures, thermal movement of PEEK molecules improved and accordingly, the relative orientation of PEEK rings are changed. For three-chain PEEK molecules, increase in friction force is slightly higher than four and five-chain PEEK molecules. Since the smallest chain length remains more align with the graphene sheet than others when temperature is increased.

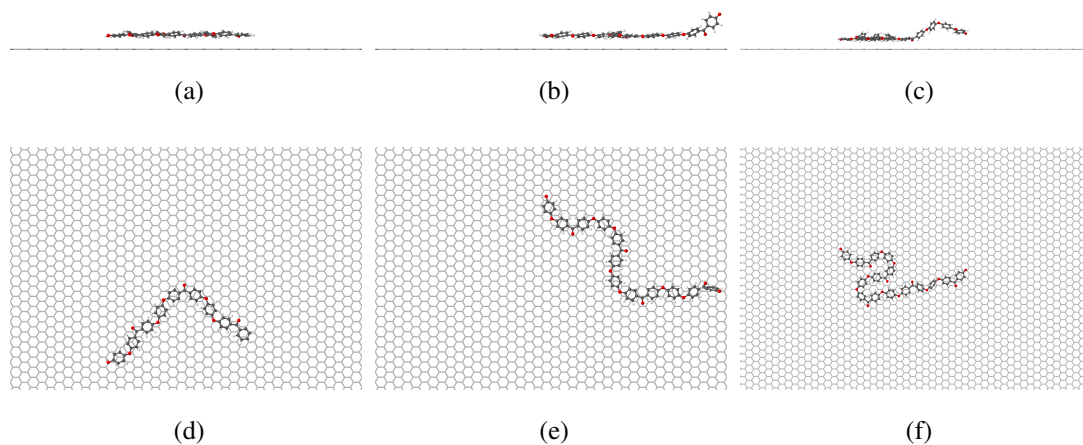


Figure 3.26: Snapshots of N-chain PEEK molecules while sliding with a velocity of 1 m/s at 1K a) 3 PEEK, (b) 6 PEEK and (c) 9 PEEK on graphene on graphene

CHAPTER 4

CONCLUSION

In this thesis, we studied the interface characteristics between graphene and PEEK. Because graphene has remarkable mechanical properties, it is used in polymer matrices as a reinforcement.

In chapter 3, we studied the adsorption energies between graphene and PEEK from its subunits to different length chains. The purpose of preliminary study was to understand the driving forces between adsorption geometries of the full monomer by looking at the details. Afterwards, full PEEK monomer is studied in DFT and MD. In MD simulations, ReaxFF potential is used at 0K and the results are in a good agreement with the DFT results. Then, we continued the interfaces studies with different PEEK chain lengths at different temperatures. From these simulations, we conclude that adsorption energies at different temperatures depend on how polymer folds onto themselves and generally, increasing temperature causes a decrease in adsorption energies. Also, we studied the effects of sliding of PEEK on graphene as a function of velocity, temperature and chain length. Results showed that increasing chain length decreases the friction forces as a consequence of folding. Furthermore, increasing temperature causes an increase in friction forces because of the thermal movements of atoms.

REFERENCES

- [1] J. Liang, Y. Huang, Y. Ma, Z. Liu, J. Cai, C. Zhang, H. Gao and Y. Chen, "Electromagnetic Interference Shielding of Graphene/Epoxy Composites," *Carbon*, Vol. 47, No. 3, 2009, pp. 922-925.
- [2] Pang, H., Chen, C., Zhang, Y., Ren, P., Yan, D., and Li, Z. (2011). The effect of electric field, annealing temperature and filler loading on the percolation threshold of polystyrene containing carbon nanotubes and graphene nanosheets. *Carbon*, 49(6), 1980-1988.
- [3] Cobos, M., and Fernández, M. (2018). Graphene Based Poly(Vinyl Alcohol) Nanocomposites Prepared by In Situ Green Reduction of Graphene Oxide by Ascorbic Acid: Influence of Graphene Content and Glycerol Plasticizer on Properties. *Nanomaterials*, 8(12), 1013.
- [4] Rafiq, R., Cai, D., Jin, J., and Song, M. (2010). Increasing the toughness of nylon 12 by the incorporation of functionalized graphene. *Carbon*, 48(15), 4309-4314.
- [5] Zhang, H., Zheng, W., Yan, Q., Jiang, Z., and Yu, Z. (2012). The effect of surface chemistry of graphene on rheological and electrical properties of polymethylmethacrylate composites. *Carbon*, 50(14), 5117-5125.
- [6] Novoselov, K. S., Geim, A. K., Morozov, S. V., Jiang, D., Katsnelson, M. I., Grigorieva, I. V., Firsov, A. A. (2005). Two-dimensional gas of massless Dirac fermions in graphene. *Nature*, 438(7065), 197-200.
- [7] Geim, A. K. and Novoselov, K. S. (2007). The rise of graphene. *Nature Materials*, 6(3), 183-191
- [8] Kuila T, Bose S, Mishra AK, Khanra P, Kim NH, Lee JH. Chemical functionalization of graphene and its applications. *Prog Mater Sci* 2012;57(7):1061-105.

- [9] Novoselov, K. S. (2004). Electric Field Effect in Atomically Thin Carbon Films. *Science*, 306(5696), 666-669
- [10] Stankovich, S., Dikin, D. A., Dommett, G. H., Kohlhaas, K. M., Zimney, E. J., Stach, E. A., . . . Ruoff, R. S. (2006). Graphene-based composite materials
- [11] A.H. Castro Nero, F. Guinea, N.M.R. Peres, K.S. Novoselov and A.K. Geim *Rev. Mod. Phys.* 81 (2009) 109
- [12] Hohenberg, P. and Kohn, W. (1964). Inhomogeneous Electron Gas. *Physical Review*, 136(3B)
- [13] Herlach, D. M., Palberg, T., Klassen, I., Klein, S., and Kobold, R. (2016). Overview: Experimental studies of crystal nucleation: Metals and colloids. *The Journal of Chemical Physics*, 145(21)
- [14] Plimpton S., Fast Parallel Algorithms for Short-Range Molecular Dynamics, *J. Comp. Phys.*, 117, 1-19 (1995)
- [15] van Duin A. C. T., Dasgupta S., Lorant F., and Goddard III W. A., ReaxFF: A Reactive Force Field for Hydrocarbons, *Phys. Chem. A*, 105, 9393-9409 (2001)
- [16] Mckeen, L. W. (2012). High-Temperature and High-Performance Polymers. *Permeability Properties of Plastics and Elastomers*, 233-250
- [17] Gebhard, A., Hauptert, F., Schlarb, A. K. (2008). Development of nanostructured slide coatings for automotive components. *Tribology of Polymeric Nanocomposites - Friction and Wear of Bulk Materials and Coatings Tribology and Interface Engineering Series*, 439-457
- [18] Berland, K., Copper V., Lee K., Schröder E. van der Waals forces in density functional theory: a review of the vdW-DF method
- [19] Giannozzi P. et al., Quantum Espresso: a modular and open-source software project for quantum simulations of materials, *J.Phys.Condens.Matter*, 21, 395502 (2009)
- [20] Plimpton S., Fast Parallel Algorithms for Short-Range Molecular Dynamics, *J. Comp. Phys.*, 117, 1-19 (1995)

- [21] D.W., Empirical potential for hydrocarbons for use in simulating the chemical vapor deposition of diamond films, *Phys. Rev. B*, (1990)
- [22] Stuart, Steven J.; Tutein, Alan B.; Harrison, Judith A. (2000). A reactive potential for hydrocarbons with intermolecular interactions. *The Journal of Chemical Physics*. AIP Publishing. 112 (14): 6472–6486.
- [23] Tersoff, J. New empirical approach for the structure and energy of covalent systems. *Phys. Rev. B*. 37: 6991 (1988).
- [24] A.C.T. van Duin, S. Dasgupta, F. Lorant, and W. A. Goddard, ReaxFF: A reactive force field for hydrocarbons, *Journal of Physical Chemistry A* 105, 9396-9409 (2001)
- [25] Gayk, F., Ehrens, J., Heitmann, T., Vorndamme, P., Mrugalla, A., and Schnack, J. (2018). Young's moduli of carbon materials investigated by various classical molecular dynamics schemes. *Physica E: Low-dimensional Systems and Nanostructures*, 99, 215-219
- [26] Zhou, K. (2020). *Carbon nanomaterials: Modeling, design, and applications*. Boca Raton, FL: CRC Press/Taylor and Francis Group.
- [27] Srinivasan S.G., van Duin A.C. T., and Ganesh P., Development of a ReaxFF Potential for Carbon Condensed Phases and Its Application to the Thermal Fragmentation of a Large Fullerene, *J. Phys. Chem. A*, 119, 571-580 (2015)
- [28] Liu L., Yi Liu, Zybin S.V, Sun H. and Goddard W. A., ReaxFF-1g: correction of the ReaxFF reactive force field for london dispersion, with applications to the equations of state for energetic materials, *J. Phys. Chem. A*, 115, 11016-11022 (2011)
- [29] Berendsen, H. J., Postma, J. P., Gunsteren, W. F., Dinola, A., and Haak, J. R. (1984). Molecular dynamics with coupling to an external bath. *The Journal of Chemical Physics*, 81(8)
- [30] Andersen, H. C. (1980). Molecular dynamics simulations at constant pressure and/or temperature. *The Journal of Chemical Physics*, 72(4), 2384-2393

- [31] Evans, D. J., and Holian, B. L. (1985). The Nose–Hoover thermostat. *The Journal of Chemical Physics*, 83(8)
- [32] D.J. Muller, Y.F. Dufrene, Atomic force microscopy as a multifunctional molecular toolbox in nanobiotechnology, *Nat. Nanotechnol.*, 3 (2008)
- [33] Mate, C.M., McClelland, G.M., Erlandsson, R., Chiang, S.: Atomic scale friction of a tungsten tip on a graphite surface. *Phys. Rev. Lett.* 59, 1942–1945 (1987)
- [34] Born, M., and Oppenheimer, J. R. (1954). On the quantum theory of molecules. New York: Technical Library, Publication Dept., Bell Telephone Laboratories.
- [35] Papageorgiou, D. G., Li, Z., Liu, M., Kinloch, I. A. and Young, R. J. (2020). Mechanisms of mechanical reinforcement by graphene and carbon nanotubes in polymer nanocomposites. *Nanoscale*, 12(4), 2228-2267
- [36] Sun, S., Chen, S., Weng, X., Shan, F. and Hu, S. (2019). Effect of Carbon Nanotube Addition on the Interfacial Adhesion between Graphene and Epoxy: A Molecular Dynamics Simulation. *Polymers*, 11(1), 121
- [37] R. Eisenshitz and F. London, Über das Verhältnis der van der Waalsschen Kräfte zu den homöopolaren Bindungskraften, *Z. Phys.* 60, 491 (1930).
- [38] F. London, Zur Theorie und Systematik der Molekularkräfte, *Z. Phys.* 63, 245 (1930).
- [39] B. I. Lundqvist, Y. Andersson, H. Shao, S. Chan, and D. C. Langreth, Density functional theory including van der Waals forces, *Int. J. Quantum Chem.* (1995).
- [40] W. Kohn and L. J. Sham, Self-consistent equations including exchange and correlation effects, *Phys. Rev.* 140, (1965).
- [41] Zheng, W., Shen, B. and Zhai, W. Surface Functionalization of Graphene with Polymers for Enhanced Properties, *New Progress on Graphene Research*, (2013).
- [42] Thomas, L. (1975). The Calculation of Atomic Fields. *Self-Consistent Fields in Atoms*, 195-203

- [43] Cooper, V. R. Van der Waals density functional: An appropriate exchange functional. *Phys. Rev. B* 2010, 81, 161104.
- [44] Berland, K., Cooper, V. R., Lee, K., Schröder, E., Thonhauser, T., Hyldgaard, P., and Lundqvist, B. I. (2015). Van der Waals forces in density functional theory: A review of the vdW-DF method. *Reports on Progress in Physics*, 78(6).
- [45] Zheng, W., Shen, B. and Zhai, W. (2013). Surface Functionalization of Graphene with Polymers for Enhanced Properties. *New Progress on Graphene Research*
- [46] Atif, R. and Inam, F. (2016). Modeling and Simulation of Graphene Based Polymer Nanocomposites: Advances in the Last Decade. *Graphene*, 05(02), 96-142.
- [47] Grimme, S. (2011). Density functional theory with London dispersion corrections. *WIREs Computational Molecular Science*, 1(2), 211-228
- [48] Berland, K., Cooper, V. R., Lee, K., Schröder, E., Thonhauser, T., Hyldgaard, P. and Lundqvist, B. I. (2015), Van der Waals forces in density functional theory: A review of the vdW-DF method, *Reports on Progress in Physics*, 78(6)
- [49] Becke, Axel D. (2014-05-14), Perspective: Fifty years of density-functional theory in chemical physics, *The Journal of Chemical Physics*. 140 (18)
- [50] Perdew, John P.; Chevary, J. A.; Vosko, S. H.; Jackson, Koblar A.; Pederson, Mark R.; Singh, D. J.; Fiolhais, Carlos (1992), Atoms, molecules, solids, and surfaces: Applications of the generalized gradient approximation for exchange and correlation, *Physical Review B*. 46 (11): 6671–6687.
- [51] Evans, D. J. and Holian, B. L. (1985). The Nose–Hoover thermostat. *The Journal of Chemical Physics*, 83(8), 4069-4074. doi:10.1063/1.449071
- [52] A. SAMOLETOV, M. A. J. CHAPLAIN, AND C. P. DETTMANN, Thermostats for slow configurational modes, *J. Stat. Phys.* 128 (2007), 1321–1336.
- [53] Y. Baskin, L. Mayer, *Phys. Rev.* 100, 544(1955)

- [54] Li, Y., Wang, Q. and Wang, S. (2019). A review on enhancement of mechanical and tribological properties of polymer composites reinforced by carbon nanotubes and graphene sheet: Molecular dynamics simulations. *Composites Part B: Engineering*, 160, 348-361.
- [55] Sun, J. and Du, S. (2019). Application of graphene derivatives and their nanocomposites in tribology and lubrication: A review. *RSC Advances*, 9(69), 40642-40661.
- [56] Najeeb, S., Khurshid, Z., Matinlinna, J. P., Siddiqui, F., Nassani, M. Z., and Baroudi, K. (2015). Nanomodified Peek Dental Implants: Bioactive Composites and Surface Modification—A Review. *International Journal of Dentistry*, 2015, 1-7
- [57] 14, A. (2016, October 19). PEEK replaces aluminum in aerospace fuel housing. Retrieved September 22, 2020, from <https://www.plasticstoday.com/peek-replaces-aluminum-aerospace-fuel-housing>
- [58] Giannopoulos, G. I., and Kallivokas, I. G. (2014). Mechanical properties of graphene based nanocomposites incorporating a hybrid interphase. *Finite Elements in Analysis and Design*, 90
- [59] Mingchao Wang, Cheng Yan and Lin Ma (August 22nd 2012). *Graphene Nanocomposites, Composites and Their Properties*, Ning Hu, IntechOpen, DOI: Available from: <https://www.intechopen.com/books/composites-and-their-properties/graphene-nanocomposites>.
- [60] Naebe, M., Wang, J., Amini, A., Khayyam, H., Hameed, N., Li, L. H., Fox, B. (2014). Mechanical Property and Structure of Covalent Functionalised Graphene/Epoxy Nanocomposites. *Scientific Reports*, 4(1).
- [61] Georgakilas, V., Tiwari, J. N., Kemp, K. C., Perman, J. A., Bourlinos, A. B., Kim, K. S., amp; Zboril, R. (2016). Noncovalent Functionalization of Graphene and Graphene Oxide for Energy Materials, Biosensing, Catalytic, and Biomedical Applications. *Chemical Reviews*, 116(9), 5464-5519.
- [62] Daukiya, L., Seibel, J., and Feyter, S. D. (2019). Chemical modification of 2D

materials using molecules and assemblies of molecules. *Advances in Physics*: X, 4(1), 1625723.

- [63] Fornasiero, P., and Cargnello, M. (2017). Preface: Morphological, Compositional, and Shape Control of Materials for Catalysis. *Studies in Surface Science and Catalysis Morphological, Compositional, and Shape Control of Materials for Catalysis*
- [64] Frenkel, D., and Smit, B. (2001). *Understanding Molecular Simulation: From Algorithms to Applications*. Burlington: Elsevier Science.
- [65] Verlet, L. (1967). Computer "Experiments" on Classical Fluids. I. Thermodynamical Properties of Lennard-Jones Molecules. *Physical Review*
- [66] Velocity command. (n.d.). Retrieved September 28, 2020, from <https://lammmps.sandia.gov/doc/velocity.html>
- [67] Bistritzer, R., and MacDonald, A. H. (2011). Moire bands in twisted double-layer graphene. *Proceedings of the National Academy of Sciences*, 108(30), 12233-12237.
- [68] Cao, Y., Fatemi, V., Fang, S., Watanabe, K., Taniguchi, T., Kaxiras, E., and Jarillo-Herrero, P. (2018). Unconventional superconductivity in magic-angle graphene superlattices. *Nature*, 556(7699), 43-50.
- [69] Staff, S. (2019, October 30). Twisted physics: Magic angle graphene produces switchable patterns of superconductivity. Retrieved October 05, 2020, from <https://phys.org/news/2019-10-physics-magic-angle-graphene-switchable.html>
- [70] Liu, N., Pidaparti, R., and Wang, X. (2017). Mechanical Performance of Graphene-Based Artificial Nacres under Impact Loads: A Coarse-Grained Molecular Dynamic Study. *Polymers*, 9(12), 134.
- [71] Jilili, J.; Abdurahman, A.; Gülseren, O.; Schwingenschlögl, U. Non-covalent functionalization of single wall carbon nanotubes and graphene by a conjugated polymer. *Applied Physics Letters* 2014, 105, 1–6.
- [72] G.A. Tomlinson. A molecular theory of friction. *Philos. Mag. Ser. 7*, 905, 1929.

[73]] University of Hamburg. Scanning [http://www.nanoscience.de/group r/theory](http://www.nanoscience.de/group%20r/theory).
probe methods group.